UNIVERSITY OF OKLAHOMA

GRADUATE COLLEGE

SOME RESULTS ON ELLIPTIC EQUATIONS AND MODELING SEASONAL DYNAMICS OF HUMAN INFLUENZA

A DISSERTATION

SUBMITTED TO THE GRADUATE FACULTY

in partial fulfillment of the requirements for the

Degree of

DOCTOR OF PHILOSOPHY

By

SHIYUN TANG
Norman, Oklahoma
2015

SOME RESULTS ON ELLIPTIC EQUATIONS
AND MODELING SEASONAL DYNAMICS OF HUMAN INFLUENZA

A DISSERTATION APPROVED FOR THE
DEPARTMENT OF MATHEMATICS

BY

Dr. Meijun Zhu, Chair

Dr. Xiangming Xiao, Co-Chair

Dr. Li Song

Dr. John Albert

Dr. Tomasz Przebinda

Dr. Luther White

DEDICATION

to

My parents

Qingxing Tang, and

Meiying Jiang

For

Encouraging me to follow my dreams

Acknowledgements

I would like to express my deep appreciation and gratitude to my PhD advisors, Dr. Meijun Zhu and Dr. Xiangming Xiao, for their guidance, encouragement and patience throughout my graduate studies. I am appreciative to have them as my advisors.

I am also grateful to professors, Song, Albert, Przebinda and White. I thank them for serving on my committee and spending time reviewing this work. I also thank the OU Mathematics department for the financial support and the teaching and guidance of the faculty, staff and students. Without their help, this dissertation would not be possible.

Contents

List of Tables

List of Figures

Abstract

This dissertation includes two parts: the theoretical study of an elliptic equation, and the practical study regarding the seasonality of human influenza.

In the first part, we focus on the study of an elliptic equation with a nonlinear boundary conditions. We establish the non-existence and existence results with respect to the different range of a parameter. To give a sense for the abstract existence result, we provide a solution to this equation for a special parameter.

In the second part, we discuss the seasonal dynamics of human influenza. According to the interactions among climate, influenza virus and human beings, we introduce three ecological based response functions: the influenza virus transmission response to the absolute humidity, the virus survival response to the air temperature and the human susceptibility to the environment temperature. The mathematical epidemiological model (SEIRS) incorporated with these response functions enables us to estimate the seasonal variation and the double peaks pattern in the subtropical pattern, as well as the single winter peak pattern observed in the temperate region. Then, we applied the model to a couple of cities along the latitude gradient and extended our simulation results to the global scale. Our model can be used to predict different flu activity pattern all over the world and help us to explore and understand the possible mechanism of the global influenza circulation.

Part I

SOME RESULTS ON THE ELLIPTIC PARTIAL DIFFERENTIAL EQUATIONS

Chapter 1

Introduction

The Rellich-Kondrachov compactness theorem tells us, for a bounded domain U in $\mathbb{R}^n$ with C^1 boundary, when p is between 1 and n, the Sobolev space $W_p^1(U)$ is compactly embedded in the $L^q(U)$ space for q is between 1 and $p^* = \frac{np}{(n-p)}$, the p^* is called the critical power. When $p = 2$, $W_p^1(U)$ is known as the Hilbert space, and denoted as $H^1(U)$ [1].

So we have the compactness theorem for Hilbert space, $H^1(U)$ is compactly embedded in the $L^q(U)$ space, with $1 \leq q < \frac{2n}{n-2}$. In the standard variation method, we often use the compact embedding to prove the convergence of the minimizing sequence. Note that H^1 space is embedded in the L^{2^*} space but not compactly embedded.

30 years ago, Brezis and Nirenberg's work on the critical power problems gives us some interesting results [2]. Let Ω be a bounded domain in R^n, with $n \geq 3$, consider the existence of solutions to the following elliptic equation. The power $\frac{n+2}{n-2}$ is critical according to the Sobolev embedding.

$$\begin{aligned} -\Delta u &= u^{\frac{n+2}{n-2}} + \mu u \quad && \text{on } \Omega \\ u &> 0 && \text{on } \Omega \\ u &= 0 && \text{on } \partial\Omega \end{aligned} \tag{1.1}$$

The solution of the elliptic equation (1.1) corresponds to the critical point

of the functional

$$F[u] = \frac{1}{2}\int |\nabla u|^2 - \frac{n-2}{2n}\int |u|^{\frac{2n}{n-2}} - \frac{\lambda}{2}\int |u|^2. \tag{1.2}$$

Note that $\frac{n+2}{n-2}+1$ is the limit exponent of the embedding, as we mentioned before. Standard variation method with compact embedding doesn't work when we try to find the critical point of the functional (1.2).

Brezis and Nirenberg showed that

1. For $n \geq 4$, if $\lambda \in (1, \lambda_1)$, equation (1.1) has a solution, where λ_1 is the first eigenvalue of the laplacian operator;

2. for $n = 3$, the existence and non-existence results depend on the value of lambda.

There is also a well-known Pohozaev non-existence result: if the domain is star-shaped, there is no solution to the equation for $\lambda = 0$ [3].

For $n = 2$, the critical exponent becomes exponential power and the equation with critical power becomes

$$\begin{cases} -\Delta u &= \dfrac{\lambda e^u}{\int\limits_\Omega e^u}, \quad \text{in } \Omega \\ u|_{\partial\Omega} &= 0. \end{cases} \tag{1.3}$$

The corresponding functional

$$F_\lambda(u, \Omega) = \frac{1}{2\lambda}\int |\nabla u|^2 - \ln\left(\frac{1}{|\Omega|}\int\limits_\Omega e^u\right), \tag{1.4}$$

for all $u \in H^1(\Omega)$, is bounded from below only for $\lambda <= 8\pi$. If $\lambda < 8\pi$,

existence of solution can be obtained by the Moser-Trudinger inequality [4]. For $\lambda = 8\pi$, for some special domain Ω, the equation has a solution [5].

In the first part of this dissertation, we are working on a similar equation in the two dimensional special domain.

1.1 H^1 Space

Let H be a real linear space.

Definition 1.1. A mapping $(,) : H \times H \to R$ is called an *inner product* if

1. $(u, v) = (v, u)$ for all $u, v \in H$,
2. the mapping $u \mapsto (u, v)$ is linear for each $v \in H$,
3. $(u, u) \geq 0$ for all $u \in H$,
4. $(u, u) = 0$ if and only if $u = 0$.

Definition 1.2. If $(,)$ is an inner product, the associated *norm* is

$$\|u\| := (u, u)^{1/2} \quad (u \in H). \tag{1.5}$$

The *Cauchy-Schwarz* inequality states

$$|(u, v)| \leq \|u\|\|v\| \quad (u, v \in H). \tag{1.6}$$

This inequality is proved as below. Using (1.5), we easily verify (1.6) defines a norm on H.

Remark 1.3. **Proof of Cauchy-Schwarz Inequation:** Let $\epsilon > 0$ and note

$$0 \leq \|u \pm \epsilon v\|^2 = \|u\|^2 \pm 2\epsilon(u, v) + \epsilon^2\|v\|^2.$$

Consequently

$$\pm(u,v) \leq \frac{1}{2\epsilon}\|u\|^2 + \frac{\epsilon}{2}\|v\|^2.$$

Minimized the right-hand side by setting $\epsilon = \dfrac{\|u\|}{\|v\|}$, provide $\|v\| \neq 0$ [1]. If $\|v\| = 0$, we have a trivial inequality: $0 \leq \dfrac{1}{2\epsilon}\|u\|^2$.

Definition 1.4. A *Hilbert space* H is a complete normed vector space endowed with an inner product which generates the norm.

Example 1. a. Let U be an open set of $\mathbb{R}^n$, the space $L^2(U)$ is a Hilbert Space, with

$$(f,g) = \int_U fg \,\mathrm{d}x.$$

b. The Sobolev space $H^1(U)$ is a Hilbert Space, with

$$(f,g) = \int_U fg + Df \cdot Dg \,\mathrm{d}x.$$

where Df, Dg are the weakly derivatives of f and g, respectively.

Remark 1.5.

Definition 1.6. Suppose $u, v \in L^1_{loc}(U)$, and α is a multiindex. We say that v is the α^{th}*weak partial derivative of* u, written

$$D^\alpha u = v,$$

provided

$$\int_U u D^\alpha \phi \,\mathrm{d}x = (-1)^{|\alpha|} \int_U v\phi \,\mathrm{d}x,$$

for all test functions $\phi \in C_c^\infty(U)$.

Definition 1.7. The *Sobolev space*

$$W^{k,p}(U)$$

consists of all locally summable functions $u : U \to \mathbb{R}$ such that for each multi-index α with $|\alpha| \leq k$, $D^\alpha u$ exists in the weak sense and belongs to $L^p(U)$.

Note: if $p = 2$, we usually write

$$H^k(U) = W^{k,2}(U) \quad (k = 0, 1, ...)$$

$H^k(U)$ is a Hilbert space, and $H^0(U) = L^2(U)$.

Definition 1.8. Let X be a Hilbert space, a sequence $\{u_k\}_{k=1}^\infty \subset X$ *converges weekly* to $u \in X$, written

$$u_k \rightharpoonup u,$$

if

$$(u^*, u_k) \to (u^*, u)$$

for each element $u^* \in X$.

Weak compactness: Let X be a reflexive Banach space and suppose the sequence $\{u_k\}_{k=1}^\infty \subset X$ is bounded. Then there exists a subsequence $\left\{u_{k_j}\right\}_{j=1}^\infty \subset \{u_k\}_{k=1}^\infty$ and $u \in X$ such that

$$u_{k_j} \rightharpoonup u.$$

In particular, a bounded sequence in a Hilbert space contains a weakly convergent subsequence.

1.2 Compact Embedding

Definition 1.9. Let X and Y be Banach space, $X \subset Y$. We say that X is *compactly embedded* in Y, written

$$X \subset\subset Y,$$

provided

(i) $\|u\|_Y \leq C\|u\|_X (u \in X)$ for some constant C, and

(ii) each bounded sequence in X is precompact in Y.

More precisely, condition (ii) means that if $\{u_k\}_{k=1}^{\infty}$ is a sequence in X with $\sup_k \|u_k\|_X < \infty$, then some subsequence $\{u_{k_j}\}_{j=1}^{\infty} \subseteq \{u_k\}_{k=1}^{\infty}$ converges in Y to some limit u:

$$\lim_{j\to\infty} \|u_{k_j} - u\|_Y = 0.$$

Theorem 1.10. *(Eberlein-Šmulian) [6]. Let A be a subset of a Banach space X. Then for the weak topology of X the following are equivalent:*

A. The subset A is conditionally compact,

B. The subset A is conditionally sequentially compact,

C. The subset A is conditionally countably compact.

Poincaré inequality: Let U be a bounded connected, open subset of $\mathbb{R}^n$, with a C^1 boundary ∂U. Assume $1 \leq p \leq \infty$. Then there exists a constant C, depending only on n, p and U, such that

$$\|u - (u)_U\|_{L^p(U)} \leq C\|Du\|_{L^p(U)} \tag{1.7}$$

for each function $u \in W^{1,p}(U)$. Note: $(u)_U = \fint_U u dx$ = average of u over U.

Trudinger's inequality [4] Let $\Omega \in \mathbb{R}^2$ be a smooth bounded domain. There are two positive constants β_0 and C_1 (C_1 depending on the area of Ω) such that if $u \in H_0^1(\Omega)$ and $||\nabla u||_{L^2} \leq 1$, then

$$\int_\Omega e^{\beta u^2} dx \leq C_1 \tag{1.8}$$

for all $\beta \leq \beta_0$. Moreover, if $\{u_i\}_{i-1}^\infty$ is bounded in $W_0^{1,n}(\Omega)$, then up to a subsequence of i, $u_i \rightharpoonup u_0$ in $W_0^{1,n}(\Omega)$ and $\exp(nu_i) \to \exp(nu_0)$ in L^1 norm.

Theorem A [3] *Suppose Ω is a bounded domain with C^k boundary Γ, $k \in \mathbb{N}$, $1 < p < \infty$. Then $W^{k,p}(\Omega) \hookrightarrow W^{k-\frac{1}{p},p}(\Gamma) \hookrightarrow W^{k-1,p}(\Gamma)$ and both embeddings are compact.*

In particular, we have

$$H^{1,2}(\Omega) \hookrightarrow L^2(\partial\Omega)$$

compactly, for any bounded domain of class C^1.

Two dimensional sharp trace inequality [7]**:** Let Ω be a simply connected domain in $\mathbb{R}^2$ with bounded Geodesic curvature K_g. Then there exists a constant $C(\Omega)$ such that for any $u \in H^1(\Omega)$,

$$\ln \int_{\partial\Omega} e^u dS \leq \frac{1}{4\pi} \int_\Omega |\nabla u|^2 dy + \frac{1}{2\pi} \int_{\partial\Omega} K_g \cdot u dS + C(\Omega). \tag{1.9}$$

Chapter 2

A Boundary Value Problem

Let Ω be part of a ball in R^2, and Γ_1 and Γ_2 be its boundary defined as follows:

$$\Omega = \left\{(x,y)|x^2+(y+\beta)^2<1+\beta^2, y>0\right\} \tag{2.1}$$

$$\Gamma_1 = \left\{(x,y)|x^2+(y+\beta)^2=1+\beta^2, y>0\right\} \tag{2.2}$$

$$\Gamma_2 = \{-1\le x\le 1, y=0\} \tag{2.3}$$

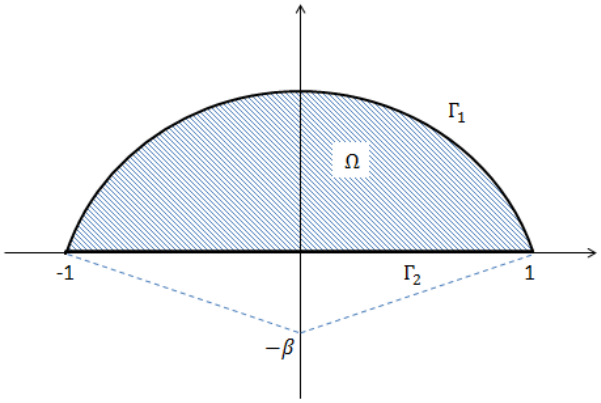

Figure 2.1: A special domain Ω

For a given positive parameter $\lambda > 0$, we consider the following equation:

$$\begin{cases} -\Delta u &= 0 & \text{on } \Omega \\ u &= 0 & \text{on } \Gamma_1 \\ \dfrac{\partial u}{\partial \upsilon} &= \lambda \dfrac{e^u}{\int\limits_{\Gamma_2} e^u \, \mathrm{d}\sigma} & \text{on } \Gamma_2 \end{cases} \tag{2.4}$$

In domain Ω, we have:

1. $|\Gamma_1| = 2\sqrt{1+\beta^2} \arcsin \dfrac{1}{\sqrt{1+\beta^2}}$

2. $\alpha = \inf\limits_{x \in \Gamma_1} (x \cdot \upsilon(x)) = \inf\limits_{(x,y) \in \Gamma_1} (x, y) \cdot \left(\dfrac{(x, y+\beta)}{\sqrt{1+\beta^2}} \right) = \sqrt{1+\beta^2} - \beta$

3. $\dfrac{2|\Gamma_1|}{\alpha} = \dfrac{4\sqrt{1+\beta^2} \arcsin \dfrac{1}{\sqrt{1+\beta^2}}}{\sqrt{1+\beta^2} - \beta}$

For any $\beta > 0$, $\dfrac{2|\Gamma_1|}{\alpha} > 2\pi$, and $\lim\limits_{\beta \to 0} \dfrac{2|\Gamma_1|}{\alpha} = 2\pi$. Here comes our main results:

Theorem 2.1. *If* $\lambda > \dfrac{2|\Gamma_1|}{\alpha} > 2\pi$, *with* $\alpha = \inf\limits_{x \in \Gamma_1} (x \cdot \upsilon(x))$, *then there is no solution to* (2.4)*; For* $0 < \lambda < 2\pi$, *there exists a solution to* (2.4).

2.1 Non-existence: $\lambda > \dfrac{2|\Gamma_1|}{\alpha}$

We first establish the corresponding Pohozaev identity for equation (2.4). Suppose u is a solution to (2.4), then we have the following:

$$
\begin{aligned}
\Delta u(\nabla u \cdot x) &= div(\nabla u(\nabla u \cdot x)) - \nabla \cdot \nabla(\nabla u \cdot x) \\
&= div(\nabla u(\nabla u \cdot x)) - \left(\frac{x}{2}\nabla|\nabla u|^2 + |\nabla u|^2\right) \\
&= div(\nabla u(\nabla u \cdot x)) - \left[div\left(\frac{x}{2}|\nabla u|^2\right) - \frac{n}{2}|\nabla u|^2\right] - |\nabla u|^2 \\
&= div(\nabla u(\nabla u \cdot x)) - div\left(\frac{x}{2}|\nabla u|^2\right) + \frac{n-2}{2}|\nabla u|^2 \qquad (2.5)
\end{aligned}
$$

Then, we integrate both sides of the above equation over Ω. Note: on Γ_1: $u = 0$, $\left|\frac{\partial u}{\partial v}\right| = |\nabla u|$, and $(\nabla u \cdot v)(\nabla u \cdot x) = |\nabla u|^2(x \cdot v)$, and on Γ_2: $(x \cdot v) = 0$. So we have:

$$
\begin{aligned}
0 &= \int_{\partial\Omega} (\nabla u \cdot v)(\nabla u \cdot x)\mathrm{d}\sigma - \frac{1}{2}\int_{\partial\Omega}(x \cdot v)|\nabla u|^2 + \frac{n-2}{2}\int_{\Omega}|\nabla u|^2\mathrm{d}x \\
&= \int_{\partial\Omega} \frac{\partial u}{\partial v}(\nabla u \cdot x)\mathrm{d}\sigma - \frac{1}{2}\int_{\partial\Omega}(x \cdot v)\left|\nabla u\right|^2\mathrm{d}\sigma \quad (\text{if } n = 2) \\
&= \frac{1}{2}\int_{\Gamma_1}\left|\frac{\partial u}{\partial v}\right|^2(x \cdot v)\mathrm{d}\sigma + \int_{\Gamma_2}\frac{\partial u}{\partial v}(\nabla u \cdot x)\mathrm{d}\sigma \qquad (2.6)
\end{aligned}
$$

On the other hand,

$$
\Delta u = div(\nabla u) \qquad (2.7)
$$

Integrate the above equation over boundary of Ω:

$$\begin{aligned} 0 = \int\limits_{\partial\Omega} \frac{\partial u}{\partial \upsilon} \mathrm{d}\sigma &= \int\limits_{\Gamma_1} \frac{\partial u}{\partial \upsilon} \mathrm{d}\sigma + \int\limits_{\Gamma_2} \frac{\partial u}{\partial \upsilon} \mathrm{d}\sigma \\ &= \int\limits_{\Gamma_1} \frac{\partial u}{\partial \upsilon} \mathrm{d}\sigma + \int\limits_{\Gamma_2} \lambda \frac{e^u}{\int\limits_{\Gamma_2} e^u \, \mathrm{d}\sigma} \mathrm{d}\sigma \\ &= \int\limits_{\Gamma_1} \frac{\partial u}{\partial \upsilon} \mathrm{d}\sigma + \lambda \end{aligned} \tag{2.8}$$

Let $I_1 = \dfrac{1}{2} \displaystyle\int\limits_{\Gamma_1} \left| \frac{\partial u}{\partial \upsilon} \right|^2 (x \cdot \upsilon) \mathrm{d}\sigma, I_2 = \int\limits_{\Gamma_2} \frac{\partial u}{\partial \upsilon} (\nabla u \cdot x) \mathrm{d}\sigma,$ then from (2.6) $I_1 + I_2 = 0.$

Using boundary condition for I_2 (we write $\nabla u = (u_1, u_2)$), we have

$$\begin{aligned} I_2 &= \int\limits_{\Gamma_2} \frac{\partial u}{\partial \upsilon} (\nabla u \cdot x) \mathrm{d}\sigma \\ &= \int\limits_{\Gamma_2} \lambda \frac{e^u}{\int\limits_{\Gamma_2} e^u \, \mathrm{d}\sigma} (u_1, u_2) \cdot (x_1, x_2) \mathrm{d}\sigma \\ &= \frac{\lambda}{\int\limits_{\Gamma_2} e^u \, \mathrm{d}\sigma} \int\limits_{(-1,1)} e^u (u_1 x_1) \mathrm{d}x_1 \\ &= \frac{\lambda}{\int\limits_{\Gamma_2} e^u \, \mathrm{d}\sigma} \left(x_1 e^u \Big|_{-1}^{1} - \int\limits_{\Gamma_2} e^u \mathrm{d}\sigma \right) \\ &= \lambda \left(\frac{|\Gamma_2|}{\int\limits_{\Gamma_2} e^u \, \mathrm{d}\sigma} - 1 \right) \end{aligned} \tag{2.9}$$

$$
\begin{aligned}
\lambda > \lambda\left(1-\frac{|\Gamma_2|}{\int\limits_{\Gamma_2} e^u \,\mathrm{d}\sigma}\right) &= -I_2 = I_1 \\
&= \frac{1}{2}\int\limits_{\Gamma_1} |\frac{\partial u}{\partial \upsilon}|^2 (x\cdot\upsilon)\mathrm{d}\sigma \qquad\qquad \alpha = \inf_{x\in\Gamma_1}(x\cdot\upsilon(x)) \\
&\geq \frac{\alpha}{2}\int\limits_{\Gamma_1} |\frac{\partial u}{\partial \upsilon}|^2 \mathrm{d}\sigma \qquad\qquad \text{Hölder inequality} \\
&\geq \frac{\alpha}{2}\left(\int\limits_{\Gamma_1}\frac{\partial u}{\partial \upsilon}\mathrm{d}\sigma\right)^2\left(\int\limits_{\Gamma_1} 1^2\mathrm{d}\sigma\right)^{-1} \qquad\qquad \text{by (2.8)} \\
&\geq \frac{\alpha}{2}(-\lambda)^2|\Gamma_1|^{-1}
\end{aligned}
$$

This implies: $\lambda < \dfrac{2|\Gamma_1|}{\alpha}$, which yields the non-existence result.

2.2 Existence: $0 < \lambda < 2\pi$

Let

$$F_\lambda[u] = \frac{1}{2}\int\limits_\Omega |\nabla u|^2 \mathrm{d}x - \lambda \ln \int\limits_{\Gamma_2} e^u \mathrm{d}\sigma \tag{2.10}$$

$$D = \left\{ u \in H^1 \,\middle|\, u|_{\Gamma_1} = 0 \right\} \tag{2.11}$$

We shall prove the existence by showing that $\inf\limits_{u\in D} F_\lambda[u]$ is attained. In fact, if there exists a function $u \in D$, such that $F_\lambda[u] = \inf\limits_{v\in D} F_\lambda[v] = \xi$, then for any $\varphi \in D$,

$$\int\limits_\Omega \nabla u \nabla\varphi - \frac{\lambda}{\int\limits_{\Gamma_2} e^u \mathrm{d}\sigma}\int\limits_{\Gamma_2} e^u\varphi \mathrm{d}\sigma = 0 \tag{2.12}$$

Thus u is a weak solution to the following differential equation:

$$\begin{cases} -\Delta u &= 0 & \text{on } \Omega \\ u &= 0 & \text{on } \Gamma_1 \\ \dfrac{\partial u}{\partial \upsilon} &= \dfrac{\lambda e^u}{\int\limits_{\Gamma_2} e^u \,\mathrm{d}\sigma} & \text{on } \Gamma_2 \end{cases} \tag{2.13}$$

To prove the existence for the minimizer to $\inf\limits_{u\in D} F_\lambda[u]$, we first show $\xi \geq C > -\infty$.

Applying Sobolev trace inequality (1.9) to our case, we have: for any $v \in C^1(\overline{\Omega})$, that

$$\ln \int\limits_{\Gamma_2} e^v \mathrm{d}\sigma \leq \frac{1}{4\pi} \int\limits_{\Omega} |\nabla v|^2 \mathrm{d}x + C_0 \tag{2.14}$$

$$\begin{aligned} F_\lambda[u] &= \frac{1}{2} \int\limits_{\Omega} |\nabla u|^2 \mathrm{d}x - \lambda \ln \int\limits_{\Gamma_2} e^u \mathrm{d}\sigma \\ &= \frac{4\pi}{2} \left\{ \frac{1}{4\pi} \int\limits_{\Omega} |\nabla u|^2 \mathrm{d}x - \ln \int\limits_{\Gamma_2} e^u \mathrm{d}\sigma \right\} + (2\pi - \lambda) \ln \int\limits_{\Gamma_2} e^u \mathrm{d}\sigma \end{aligned} \tag{2.15}$$

First we want to show $F_\lambda[u]$, for any $u \in D$ is bounded from below.

1. : $0 < \lambda < 2\pi$

   If $\ln \int\limits_{\Gamma_2} e^u \mathrm{d}\sigma > 0$, from (2.15), $F_\lambda[u] > -C_0 + (2\pi - \lambda) \ln \int\limits_{\Gamma_2} e^u \mathrm{d}\sigma > -C_0$;

   if $\ln \int\limits_{\Gamma_2} e^u \mathrm{d}\sigma < 0$, from (2.14), $F_\lambda[u] > \dfrac{1}{2} \int\limits_{\Omega} |\nabla u|^2 \mathrm{d}x \geq 0$.

2. : $\lambda = 2\pi$

   From (2.15), $F_\lambda[u] > -C_0$.

When $\lambda \leq 2\pi$, $\inf\limits_{u\in D} F_\lambda[u] > C_1 > -\infty$ exists.

Second we need to show the convergence of minimizing sequence.

Let $u_n \subset D$ be a minimizing sequence of $\inf_{u\in D} F_\lambda[u]$. For n large enough, there exist finite number C_2, s.t. $C_1 < F_\lambda[u_n] < C_2$.

$$\begin{aligned}\frac{1}{2}\int_\Omega |\nabla u_n|^2 \mathrm{d}x &< C_2 + \lambda \ln \int_{\Gamma_2} e^{u_n} \mathrm{d}\sigma \\ &\leq C_2 + \lambda \left\{ \frac{1}{4\pi}\int_\Omega |\nabla u_n|^2 \mathrm{d}x + C_0 \right\} \qquad \text{From (2.14)}\end{aligned}$$

Then if $\lambda < 2\pi$

$$\begin{aligned}\left\{\frac{1}{2} - \frac{\lambda}{4\pi}\right\}\int_\Omega |\nabla u_n|^2 \mathrm{d}x &< C_2 + \lambda C_0 \\ \int_\Omega |\nabla u_n|^2 \mathrm{d}x &< \frac{C_2 + \lambda C_0}{\frac{1}{2} - \frac{\lambda}{4\pi}} \end{aligned} \tag{2.16}$$

Note that $\|u_n\|^2_{H^1} = \int_\Omega |\nabla u_n|^2 \mathrm{d}x + \int_\Omega u_n^2 \mathrm{d}x$ is bounded. Thus, by weakly compactness, up to a subsequence, $u_n \rightharpoonup u^*$ weakly, for some $u^* \in D$; and $\|u^*\|_{H^1} \leq \underline{\lim} \|u_n\|_{H^1}$.

Also we can get the estimation of the second term in $F_\lambda[u]$ by the similar argument.

$$\begin{aligned}\lambda \ln \int_{\Gamma_2} e^u \mathrm{d}\sigma &\geq \frac{1}{2}\int_\Omega |\nabla u|^2 \mathrm{d}x - C_2 \\ &\geq -C_2 \end{aligned} \tag{2.17}$$

$$\begin{aligned}\lambda \ln \int_{\Gamma_2} e^u \mathrm{d}\sigma &\leq \frac{1}{2}\int_{\Omega} |\nabla u|^2 \mathrm{d}x - C_1 \\ &\leq \frac{1}{2}\frac{C_2 + \lambda C_0}{\frac{1}{2} - \frac{\lambda}{4\pi}} - C_1 \end{aligned} \tag{2.18}$$

So $\lambda \ln \int_{\Gamma_2} e^u \mathrm{d}\sigma$ is bounded when $\lambda < 2\pi$.
Finally, we come to our existence result:

$$\begin{aligned} F_\lambda[u^*] &= \frac{1}{2}\|\nabla u^*\|^2 - \lambda \ln \int_{\Gamma_2} e^{u^*} \mathrm{d}\sigma \\ &\leq \left\{ \liminf_{n\to\infty} \frac{1}{2}\|\nabla u_n\|^2 - \limsup_{n\to\infty} \lambda \ln \int_{\Gamma_2} e^{u_n} \mathrm{d}\sigma \right\} \\ &\quad + \limsup_{n\to\infty} \lambda \ln \int_{\Gamma_2} e^{u_n} \mathrm{d}\sigma - \lambda \ln \int_{\Gamma_2} e^{u^*} \mathrm{d}\sigma \\ &\leq \lim_{n\to\infty} \left\{ \frac{1}{2}\|\nabla u_n\|^2 - \lambda \ln \int_{\Gamma_2} e^{u_n} \mathrm{d}\sigma \right\} \\ &\quad + \limsup_{n\to\infty} \lambda \ln \int_{\Gamma_2} e^{u_n} \mathrm{d}\sigma - \lambda \ln \int_{\Gamma_2} e^{u^*} \mathrm{d}\sigma \\ &= \xi + \limsup_{n\to\infty} \lambda \ln \int_{\Gamma_2} e^{u_n} \mathrm{d}\sigma - \lambda \ln \int_{\Gamma_2} e^{u^*} \mathrm{d}\sigma \end{aligned} \tag{2.19}$$

Since $\|\nabla u_n\|_{H^1}$ is bounded in D, according to the Poincaré inequality,

$$\|u_n\|_{L^p} \leq C_p \|\nabla u_n\|_{L^p},$$

for $1 \leq p \leq \infty$, so $\{u_n\}$ is compact in L^p. Now we only need to show the

following limit obtained:

$$\limsup_{n\to\infty} \lambda \ln \int_{\Gamma_2} e^{u_n} \mathrm{d}\sigma \to \lambda \ln \int_{\Gamma_2} e^{u^*} \mathrm{d}\sigma \tag{2.20}$$

According to [7]Page 36: H^1 is compact embedding in L^2, $u_n \rightharpoonup u^*$ in $H^1(\Omega)$ and $e^{\beta u_n} \to e^{\beta u^*}$ in $L^1(\Omega)$ for any positive β by Trudinger inequality.

For any $1 < p < 2$,

$$\begin{aligned} \int_\Omega |\nabla e^{\beta u_n}|^p &= \int_\Omega |e^{\beta u_n} \beta \nabla u_n|^p \\ &\le \beta^p \Big(\int_\Omega e^{\frac{2p\beta}{2-p} u_n}\Big)^{(2-p)/2} \Big(\int_\Omega |\nabla u_n|^2\Big)^{p/2} \\ &\le c\Big(\int_\Omega |\nabla u_n|^2\Big)^{p/2} \\ &\le C, \end{aligned}$$

thus $\{e^{\beta u_n}\}$ is a bounded sequence in $W^{1,p}(\Omega)$. Therefore, for any $\beta > 0$ and $1 < p < 2$, by the compact embedding, $e^{\beta u_n} \to e^{\beta u^*}$ in $L^p(\partial\Omega)$ upto subsequence. Hence $e^{\beta u_n} \to e^{\beta u^*}$ in $L^1(\partial\Omega)$ for any $\beta > 0$. So, (2.20) holds.

Now we have our conclusion: When $0 < \lambda < 2\pi$, $\inf\limits_{u\in D} F_\lambda[u]$ is attained, which leads to the existence result. For $2\pi \le \lambda \le \dfrac{2|\Gamma_1|}{\alpha}$ is still under discussion.

2.3 A Special Case

In this section, we will show the existence to equation (2.4) for a special $\lambda < 2\pi$ by constructing a precise solution.

For a given $\beta > 0$, let $\lambda = 4 \arctan \dfrac{1}{\beta} < 2\pi$. We claim that

$$u(x, y) = \ln \frac{1 + \beta^2}{x^2 + (y + \beta)^2} \tag{2.21}$$

solves the partial differential equation (2.4).

In fact, easy to see that $\Delta u = 0$ for $(x, y) \in \Omega$, and $u = 0$ for $(x, y) \in \left\{(x, y)|x^2 + (y + \beta)^2 = 1 + \beta^2\right\}$.

On Γ_2: Since

$$e^u|_{y=0} = \frac{1 + \beta^2}{x^2 + \beta^2},$$

and

$$\int_{\Gamma_2} e^u \mathrm{d}\sigma = \int_{-1}^{1} \frac{1 + \beta^2}{x^2 + \beta^2} \mathrm{d}x = \frac{2(1 + \beta^2)}{\beta} \arctan \frac{1}{\beta},$$

we have

$$\left.\frac{\partial u}{\partial \upsilon}\right|_{\Gamma_2} = \left.\frac{\partial u}{\partial(-y)}\right|_{y=0} = \frac{2\beta}{x^2 + \beta^2} = \left.\frac{2\beta}{1 + \beta^2} e^u\right|_{\Gamma_2} = 4 \arctan \frac{1}{\beta} \left.\frac{e^u}{\int_{\Gamma_2} e^u \mathrm{d}\sigma}\right|_{\Gamma_2}.$$

Part II

SPATIAL PATTERN AND SEASONAL DYNAMICS OF HUMAN INFLUENZA IN GLOBAL SCALE

Chapter 3

Introduction

Seasonal influenza (flu) is one of the most significant respiratory infectious diseases in human population. According to World Health Organization (WHO, 2014) report, seasonal influenza was associated with 3 to 5 million severe illness cases and 250,000 to 500,000 human deaths per year over the world [8]. Influenza occurs globally with an annual attack rate estimated at 5% - 10% in adults and 20% - 30% in children. Flu causes a heavy burden not only on public health but also on the economy [9]. The annual economic costs of influenza varied from $13.9 thousand to $957.5 million across US counties (based on Census 2010), with a median of $2.47 million [10].

Recently, many research works focus on the relationship among weather, climate and influenza [9]. The distinct seasonality of influenza suggests a climate connection, but the wide range of methodologies used to explore this connection makes it difficult to elucidate a definitive relationship. In general, studies of influenza can be divided into two aspects:

1. laboratory-based studies on viral etiology and host susceptibility and how they vary under different environmental conditions;

2. epidemiological studies relating large-scale morbidity and mortality patterns to various climate signals and atmospheric conditions.

The seasonal dynamics of influenza in the temperate regions, which is characterized by a strong peak in cold winter months, are well documented [11],

but not well understood [12]. Many models and mechanisms (risk factors) have been proposed to explain the seasonal dynamics of influenza in the temperate regions, ranging from intrinsic oscillation [13] to exogenous driving factors, e.g., relative humidity, specific humidity, air temperature, and ultra violet radiation [9, 14, 15, 16]. Humidity seems to be the primary factors that produce the winter activity in the North temperate region [18]. In the tropic and subtropical regions where hot and humid condition is predominant, the flu activity patterns are various, from single distinct winter peak, semi-annual peaks to persistency, which have weak relation to the latitude gradient and social activities [19]. Particularly, In the East and Southeast of Asia, several cities experience the semi-annual peaks, which cannot be explained by any single risk factor.

3.1 Human Influenza

There are two main types of influenza viruses: type A and B. Both types routinely spread in the human populations and are responsible for human flu epidemics each year. Influenza A can be divided into different subtypes depending on the genes that make up the surface proteins, hemagglutinin (H) and neuraminidase (N). Both types can be further broken down into different strains. Over the course of a flu season, different types of both viruses and different subtypes of influenza A circulate and cause illness. Small changes happen in the viruses over time, so that human immune system may not recognize the new virus, and because of this reinfection occurs. This is the main reason why most people will get flu more than once in a year.

Most experts believe that flu transmission is caused by the droplets made when people with flu talk, sneeze, and cough. People may be able to pass

on flu before they know they are sick. The contagiousness begins one day before symptoms develop and remains up to 5-7 days after becoming sick [12]. Yearly influenza epidemics can seriously affect all populations, but the highest risk of complications occur among children younger than age 2 years, adults aged 65 years or older, pregnant women, and people of any age with certain medical conditions. Winter is the time for flu, but the exact time and seasonal duration varies. In the northern hemisphere, flu outbreaks can happen as early as October, and end as late as April. But most of the time, flu activity peaks after January. In the subtropical region, the flu happens more than once a year. In the tropic, flu activity is associated with the rainy season.

3.2 Influenza Circulation Related to the Climate and Weather

During epidemiological circulation, the climate and weather effects are involved in the viral transmission, host susceptibility, and virulence of the flu virus, which are considered to be the major epidemiological components of influenza pathways that facilitate and maintain the cycle of disease. Basically, the climate- and weather- effects are involved in the viral transmission, host susceptibility, and virulence of the flu. Until now, research on the environmental effects of influenza transmission has focused primarily on environment humidity and temperature in laboratory – controlled settings [9]. The humidity affects the size of the respiratory particles in the 3 main types of the viral transmission: droplet, contact, and airborne [20]. When the air is dry, the particles shrink to a smaller size and can stay in the air for a longer time and travel longer distances. A recent study on guinea pigs found that the relative role of contact and airborne transmission may be sensitive to changes in air temperature [21]. High

temperatures block airborne transmission of the influenza virus but not contact transmission [12]. When considering the combined effects of environment humidity and temperature on influenza transmission, it appears that airborne transmission is more sensitive to changes in these variables than contact and droplet modes [9].

At the core of the debate over the causal mechanisms responsible for the seasonality of many infectious diseases is the role of population immunity and overall susceptibility to infection. One of the pioneers in this area of study was Edgar Hope-Simpson [22, 23]. Hope-Simpson identified the seasonal stimulus as a deficiency in vitamin D levels because of seasonal reductions in exposure to ultra-violet (UV) radiation. Low levels of vitamin D have been shown to impair the body's antimicrobial peptide system, which is responsible for regulating the immune response [23, 24].

In addition to the innate immunity of healthy individuals, the host response to infection with respect to viral shedding has been shown to be sensitive to changes in ambient temperature. In the experimental studies involving viral transmission between guinea pigs, researchers found that infected hosts exposed to lower ambient temperatures shed significantly higher quantities of viral particles than those exposed to higher temperatures. Moreover, the period of peak shedding was extended by as many as 2 days when infection occurred at 5^oC compared with 20^oC [21].

Besides factors such as transmission cycles and host susceptibility, the ability of the influenza virus to cause infection (virulence) is also important in the context of disease ecology and the seasonality of infection. Viral strains with a history of high infectivity, such as the H5N1 avian influenza, may indeed override any innate or adaptive immunity (including vaccination) regardless of

environmental conditions. Virulence of the circulating viral strain often varies from year to year.

3.3 Spatial Pattern of Influenza Activity

The fact that temperature and humidity fluctuate with the seasons in temperate climates, and that influenza epidemics exhibit a distinct seasonality in these areas, suggests the airborne route is the dominant mode of transmission in temperate regions [12]. The relative lack of seasonality in influenza prevalence in tropical regions, where there is less variability in temperature and humidity, suggests that contact and droplet modes are dominant there [25]. Further, the primary source for sporadic and isolated outbreaks that sometimes occur in temperate regions during the summer may be contact and droplet transmissions operating in optimal microclimate conditions (i.e., conditions present in tropic areas).

Past observations that influenza epidemics occur in the winter across temperate climates, combined with insufficient knowledge about the epidemiology of influenza in the tropics, led to the perception that cool and dry conditions were a necessary, and possibly sufficient, driver of influenza epidemics. Recent reports of substantial levels of influenza virus activity and well-defined seasonality coincident with rainy season in tropical regions [26, 27], where warm and humid conditions often persist year-round, have rendered previous hypotheses insufficient for explaining global patterns of influenza [14]. A recently work even observed a double-peak influenza activity in the subtropical region [28], especially some cities along southeast Asia [19].

The macroscopic study is necessary to describe the mechanism under the

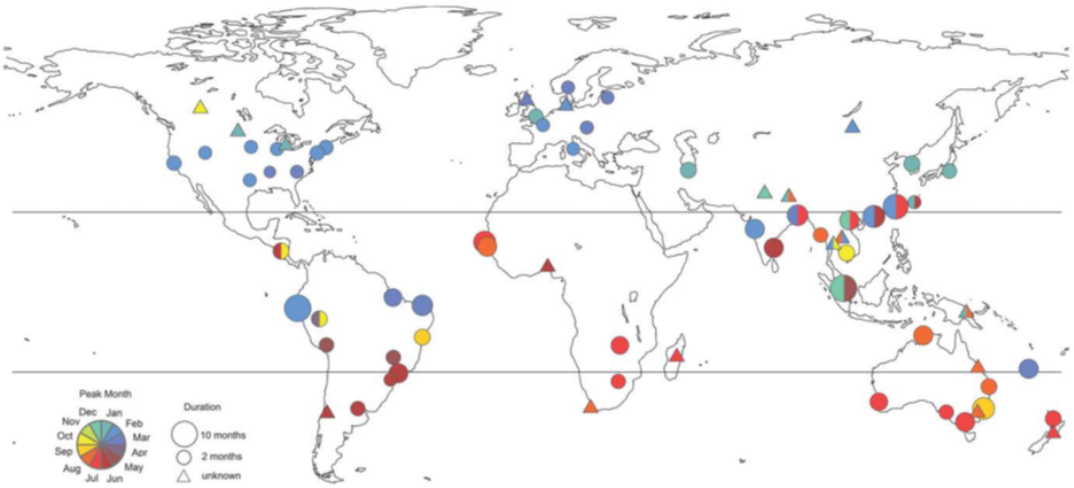

Figure 3.1: Global map of influenza peak timing and epidemic duration (n = 77 locations) [19]. Colors illustrate timing of peak influenza activity, based on the bottom left key, while size of the circles is proportional to epidemic duration. For independent observations for the same location, an average was taken. For studies that did not provide enough information to estimate duration, a triangle is shown. Circles filled out with more than one color represent locations experiencing semi-annual peaks of virus activity (methods). In the temperate region, single peak activity is predominant; semi-annual peaks appears around the subtropical region, especially southeast Asia; in the tropic, multiple peaks and long period of flu circulation suggest a high activity background

large scale climate effect to the influenza seasonality. In ecology, there is a source-sink model for many species populations. A large fraction of the individuals may regularly occurs in "sink" habitats, where within-habitat reproduction is insufficient to balance local mortality; nevertheless, species populations may persist in such habitats, being locally maintained by continued immigrating from more-productive "source" areas nearby [29]. Rambaut et.al. propose a source-sink model for the global ecology of influenza A virus. Continual gene flow from a common source population (which they suggested is on tropical region) provides the viruses that ignite each epidemic in human populations of the Northern and Southern Hemispheres [30].

3.4 Scientific Questions to be Addressed, Hypotheses and Objectives

The mechanism of flu circulation is still under discussion. The winter peak observed in the temperate region is well document but not well understood. The models consist of periodical parameters that can produce the seasonal dynamics in a calender year, but are not able to predict the variations among different years. Most studies of local epidemic can only explain the behavior locally, but are not able to extend their result to a wider range. In this study, we constructed risk factors including influenza virus transmission and virus survival as well as human susceptibility, and successfully reproduced the Winter peak in Beijing (temperate zone) and the Summer/Winter peaks in Hong Kong (tropical zone) [31]. We also considered the case of multiple cities and found a simple spatial pattern throughout the world. In the following, we applied the same model to the globe, to see if the influenza activity pattern changes continuously across the latitude/longitude gradient.

3.4.1 Hypothesis

In the subtropical/tropic region, semiannual peaks, also known as the winter – summer peaks pattern, cannot be simulated only by a single factor like humidity which effectively predicts the winter peak in the temperate zone [18]. We propose the following hypothesis to estimate the flu activity in the East Asia:

1. The observed temporal dynamics of influenza A in Hong-Kong cannot be explained by the influence of the specific humidity on the influenza virus transmission alone;

2. Changes in human susceptibility to virus infection with weather factors, such as environmental temperature and radiation, play a role in determining the seasonal dynamics of influenza;

3. The two-peak pattern of seasonal influenza A dynamics observed in Hong Kong can be reproduced by the major risk factors:

   (a) influenza transmission through aerosols (IVT),

   (b) influenza virus survival (IVS) in the environment,

   (c) and human susceptibility (HS) to infection;

4. The one-peak pattern observed in the dynamics of influenza A in temperate regions can also be reproduced under (3).

3.5 Main Results and Applications

According to the weather – climate – influenza relation, we introduced three ecological based response functions. The SEIRS models, with these response functions, are able to produce the seasonality of human influenza in the north

temperate region, as well as in the subtropical and tropical regions. Then, we applied our model to a wide range of latitude by choosing multiple cities along the latitude gradient.

The results of most cities we picked had quite similar seasonal pattern and peaking time as Google Flu Trend data. Then, we were able to depict and reproduce the influenza circulation throughout the world by our revised SEIRS model coupling with the global climate data and population data. This global simulation result resembles the observation in peak patterns. The result not only enhances the result about the temperate, subtropical and tropical zones, but also support the source-sink global ecology hypothesis proposed by Rambaut [30]. Even more, we identified polar and equatorial regions as sources other than one tropic source in his hypothesis. With respect to our work, there are three areas: North cold zone, South cold zones and tropic region which satisfied the criteria of the influenza source.

This chapter briefly introduces the key factors of the human influenza, seasonality and spatial distribution of flu activity, as well as driven factors of the oscillation. The following chapters introduce the mathematical/epidemic models with response functions, provide the source and detail information of the weather data we used in the simulation, and describe our simulation design in different scenarios. Finally, the main results with statistical analysis, comparison and discussion will be presented.

Chapter 4

Method

4.1 Epidemiological Models

4.1.1 Compartment Models

In an acute infection, assuming the pathogen causes illness for a period of time following by immunity, we can suppose individuals are either susceptible to infection, infectious or recovered (previously infected and consequently immune). Under this assumption, the population can be divided into compartment with respect to their health status: Susceptible, infected and recovered. Then we can mathematically describe the population-level epidemic dynamics with so-called S-I-R models, which were studied by Kermack and Mckendrick in the early 1990s. These models are known as compartmental models in epidemiology, and serve as a basis mathematical framework for understanding the complex dynamics of these systems, which hope to model the main characteristics of the system [32, 33].

Once one is able to model an infectious pathogen with compartmental models, one can predict the various properties of the pathogen spread, for example the prevalence (total number of infected from the epidemic) and the duration of the epidemic. Also, one can understand how different situations may affect the outcome of the epidemic, e.g., what is the best technique for issuing a limited number of vaccines in a given population.

In the simplest case (ignore population demography births, deaths and migration), there are two transitions: S $\rightarrow$ I and I $\rightarrow$ R. The second one describes the infected individual fights off the infection and move to the recovered class. The amount of the time spent in the infectious class ("the infectious period") distributed around around some mean value, which can be estimated from the clinical data. In the modeling perspective, the probability of an individual moving from I to R is dependent on how long they have been in the I class.

The progression from S to I clearly involves disease transmission, which is determined by 3 district factors: the prevalence of infected, the underlying population contact structure, and the probability of transmission given contact. For a directly transmitted pathogen, there has to be contact between susceptible and infected individuals and the probability of this happening is determined by the respective levels of S and I, as well as the inherent contact structure of the host population. Finally, we need to take into account the likelihood that a contact between a susceptible and infectious person results in transmission. These conceptual descriptions of the model can be represented by a flow diagram, using black arrows to show the movement between the S and I classes and the I and R classes.

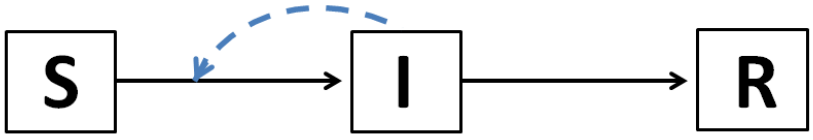

Figure 4.1: Compartment model. The black arrows indicate the transmission of Individuals from Susceptible (S), to Infected (I), and Infected (I) to Recovered (R) class. The dash arrow represent the contact of S and I class that causes the S class move to the I class.

The letters can also represent the number of individuals under the responding health statuses at a specific time t, denoted as $S(t)$, $I(t)$, and $R(t)$. Then during the unit time, average number of the adequate contacts that cause the infections denoted by β. The total number of adequate contacts that made by single susceptible individual with infected becomes $\beta\frac{I(t)}{N}$; the total number of new cases in the unit time is $\beta\frac{I(t)}{N}S(t)$. Let N denote the total population, and γ be the probability that Infected class move to the Recovered class. Then the mathematical model (SIR) comes out:

$$\begin{cases} \dfrac{dS(t)}{dt} &= -\dfrac{\beta S(t)I(t)}{N} \\ \dfrac{dI(t)}{dt} &= \dfrac{\beta S(t)I(t)}{N} - \gamma I(t) \\ \dfrac{dR(t)}{dt} &= \gamma I(t) \end{cases} \tag{4.1}$$

If the initial fraction of susceptibles $S(0)/N < \dfrac{\gamma}{\beta}$, then $\dfrac{dI}{dt} < 0$ and the infection "die out". The inverse of this fraction is called the basic reproductive ratio and is one of the most important quantities in epidemiology. We will discuss it later.

4.1.2 SEIRS Models

SEIRS models, one type of the deterministic compartmental models, are common used to describe the dynamical process of the influenza circulation in the human population. In the model, the human population is divided into 4 classes (compartments): S(susceptible), E(exposed), I(infectious) and R(recovered)

during the flu circulation. The following formula describes this model:

$$\begin{cases} \frac{dS(t)}{dt} &= \lambda N(t) - \mu S(t) - \beta(t)\frac{S(t)I(t)}{N(t)} + \rho R(t) \\ \frac{dE(t)}{dt} &= \eta E(t) - (\mu+\gamma)I(t) \\ \frac{dI(t)}{dt} &= \beta(t)\frac{S(t)I(t)}{N(t)} - (\mu+\eta)E(t) \\ \frac{dR(t)}{dt} &= \gamma I(t) - (\mu+\rho)R(t) \end{cases} \tag{4.2}$$

where $N(t) = S(t)+E(t)+I(t)+R(t)$ is the total population. Figure 4.2 shows the influenza virus circulation inside the human population.

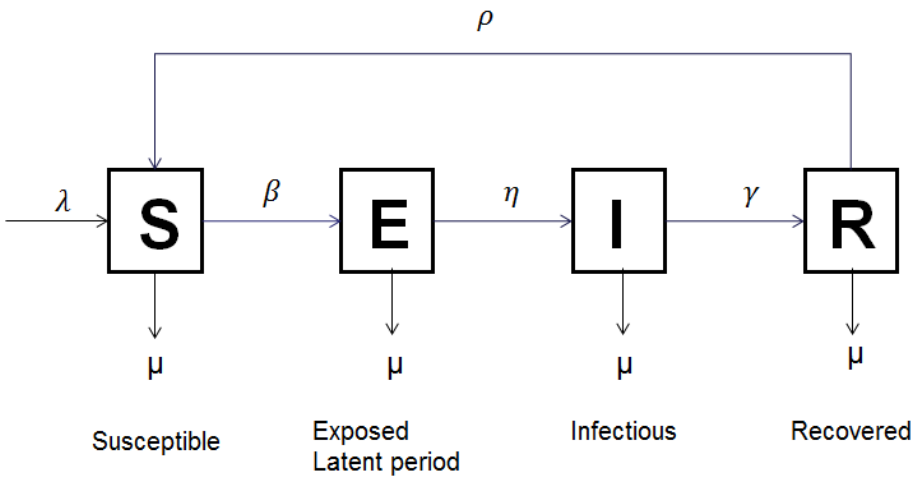

Figure 4.2: Influenza circulates inside the human population. Susceptible (S), Exposed (E), Infected (I) and Recovered (R) are the four health status during an epidemic. The arrows indicate the transmission of individuals among the four class. The 4 parameters β, η, γ, ρ are the transmission rate from one class to the successive class, respectively. λ and μ are the birth and death per capita.

As a simplification, the total population N is assumed to stay the same during flu circulation procedure, which means natural birth rate equals natural death rate, represented by μ. Parameters β, η, γ and ρ describe the transmission rates between two successive classes (see Table.4.1). Rate β is the contact transmission, rate η is the rate at which latent individuals move to the infectious

class, and γ is the rate at which infectious individuals recover from illness. ρ is the average rate at which recovering individuals lose immunity and become susceptible again. The model presents the circulation of the influenza inside a human population. Since the human influenza occurs yearly with a periodical activity pattern, the convenient way to introduce a time dependent circulation is to add a time-dependent periodical function into the transmission rate $\beta(t)$ in a compartmental model [13].

$$\beta(t) = \beta_0 \times (1 + \beta_1(t) \cos 2\pi t). \tag{4.3}$$

Parameter	**Value**	**Description**	**Ref.**
η	1/2 (1/days)	Rate of transmission from exposed to infectious individual	[16, 34]
μ	3.91×10^{-5}	Mortality rate	[35]
γ	1/7 (1/days)	Recovery rate	[8, 34]
ρ	1/.5 – 1/12 (1/month)	Average rate at which individuals lose immunity	

Table 4.1: Values and ranges of transmission parameters

4.1.3 Reproduction Number R_0

There is a very important criterion of the influenza epidemics called Reproduction Number and represented by R_0. It is the number of secondary infections from a single infection in a population where all subjects are susceptible. We deduced the R_0 from our SEIR model:

$$R_0 = \frac{\beta\eta}{(\mu + \eta)(\mu + \gamma)} \tag{4.4}$$

This value essentially measures the maximum reproductive potential for an infectious disease. An outbreak occurs if and only if the reproduction number is greater than one. Under this condition more than one person will be infected by the same infected person, hence the number of infected individuals will grow exponentially and an epidemic out-break will occur. Otherwise, the disease will die out. In our model, we considered that R_0 varies from time to time, $R_0 = R(t)$, since influenza circulates year round. We had the same criteria: when $R(t) > 1$, the influenza epidemic occurs; when $R(t) < 1$, the flu disappears; when $R(t) = 1$, the disease maintains.

4.1.4 Contact Rate

The average number of direct contacts that the infectious individuals made with the susceptible individuals and pass the illness to them, is called the contact rate. We can obtain the relation between R_0 and β from the differential equation (4.2) to get the transmission rate:

$$\beta(t) = R_0(t) \times \frac{\eta}{(\mu + \eta) \times (\mu + \gamma)}. \tag{4.5}$$

The estimation of the reproduction number R_0 is between 0.8 to 4 [16]. Since the $R(t)$ changes when time changes, the contact rate is also a time dependent function.

4.2 Ecological Response Functions

In our new and novel approach to the epidemic model SEIRS (Eq.(4.2)), we propose a time-dependent reproduction number $R_0(t)$ first,

$$R_0(t) = R_{0\max} \times \frac{p(t)}{\max p(t)}. \tag{4.6}$$

where the risk probability $p(t)$ at a given time t, is a time-varying scalar for influenza virus survival, transmission and human susceptibility under changing weather and climate.

The climate factors, such as specific humidity [15, 16], air temperature [15, 16, 21] and ultra violet radiation [9, 23, 24, 36], are believed to be the driving factors of the strong influenza peak in winter in the temperate regions. Aerosol-based transmission and survival of influenza virus [15, 16] and human susceptibility to influenza are key clues to flu prevalence. We constructed three response functions–influenza virus transmission to humidity ($\mathrm{IVT_{sh}}$), virus survival to temperature (IVS_T), and human susceptibility to temperature (HS_T)–in order to describe several aspects of the risk probability [31]. Figure 4.3 gives the theoretic response of these three factors.

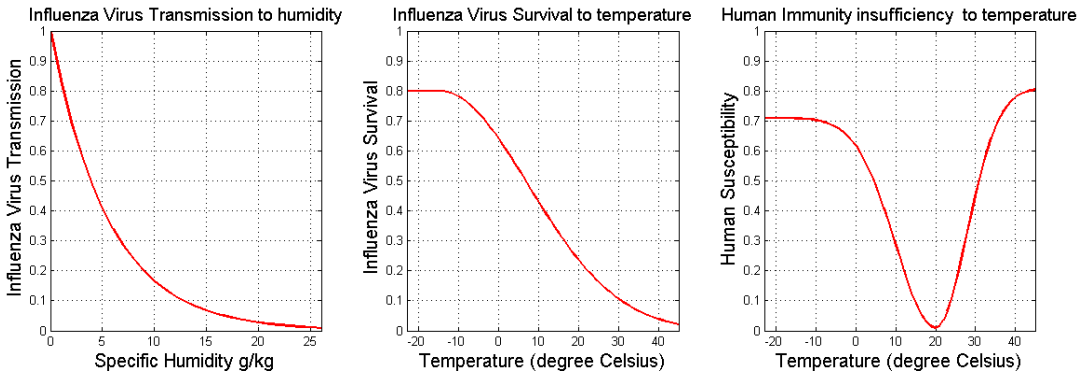

Figure 4.3: Theoretic ecological response functions.

- IVT_{sh}: From recently laboratory-based studies on viral etiology [15, 16], we defined the Gaussian type function of Influenza virus transmission with respect to specific humidity as following:

$$IVT_{\text{sh}} = 5 \times \exp\left(-\frac{(SH + SH_{\min})^2}{0.9 \times 10^{-3}}\right), \tag{4.7}$$

where SH is the specific humidity in kg of water/kg of air at time t, while $SH_{\min} = 0.04$ kg/kg, an artificial constant. This function shows how the dry air favors the virus transmission. Another way to describe this effect is proposed by Shaman (Eq.4.8), by his model, the temperate region results are well fitted with US Center of Diseases Control and Prevention(CDC) report [18].

$$IVT^{\text{s}}_{\text{sh}} = \exp\left(-180 \times SH\right), \tag{4.8}$$

- IVS_T: We constructed the function of influenza virus survival with respect to temperature change according to the data in [15, 16] as another Gaussian type function given by:

$$IVS_T = 0.8 \times \exp\left(\frac{-\left(T - T_{\min 1}\right)^2}{1000}\right), \tag{4.9}$$

where T is the air temperature in °C, while $T_{\min 1} = -15$°C. Since low temperature favors the influenza survival, as temperature increases, the survival rate drops down [9].

- HS_T: According to human physiology, human body in cold and hot condition is relatively easy to get sick. An adequate level of wintertime warmth is 21°C (70°F) for a living room, and a minimum of 18°C (64°F) for oth-

er occupied rooms, giving 24°C (75°F) as a maximum comfortable room temperature for sedentary adults [37]. Death through heat stress increase when temperature above 28°C (82°F), and at temperatures below 20°C (68°F), increased risk of death has been observed. So we suggest a U shape for human susceptibility function dependent on temperature:

$$\begin{aligned} HS_T = 0.01 \quad &+ \quad 0.7 \times \left(1 - \exp\left(-\frac{(T - T_{opt})^2}{200}\right) U_1\right) \\ &+ \quad 0.8 \times \left(1 - \exp\left(-\frac{(T - T_{opt})^2}{125}\right) U_2\right), \end{aligned} \tag{4.10}$$

with T is the air temperature in °C, and the two functions $U_i (i = 1, 2)$ are given by

$$U_1(T) = \begin{cases} 1 & \text{if } T_{\min 2} < T < T_{opt} \\ 0 & otherwise \end{cases} \tag{4.11}$$

and

$$U_2(T) = \begin{cases} 1 & \text{if } T_{opt} < T < T_{\max} \\ 0 & otherwise \end{cases} \tag{4.12}$$

with $T_{\min 2} = -25$°C, $T_{opt} = 20$°C, and $T_{\max} = 45$°C. This actually is coherent with the human physiology: human body feels not well in high or low temperature.

4.2.1 Risk Factor $p(t)$

We considered the average value of all the response functions as the risk factor $p(t)$ to produce the dominant risk factor with respect to the climate data in different areas.

$$p(t) = \frac{IVT_{sh} + IVS_T + HS_T}{3} \tag{4.13}$$

We also consider the maximum of all the possible risk factors as another choice of risk factor,

$$P(t) = \max\{IVT_{SH}, IVS_{T_{max}}, IVS_{T_{min}}, HS_{T_{max}}, HS_{T_{max}}\} \tag{4.14}$$

In the winter low temperature and low humidity dominant, in the summer hot and dry weather drives the flu activity. So we can choose the maximum of all the factors in different time to find the main effect. Also, use weekly and recent data to compare the simulation and estimation report.

Once the risk factor is obtained from all the 3 response functions, from equation (4.5) and (4.6), the contact rate $\beta(t)$ is ready for the ODE system. Since risk factor and transmission rate are both dependent on the climate factors (temperature and humidity) which are also dependent on time; ultimately, the transmission rate β become a time dependent function. Our model describes the flu circulation with respect to time.

4.2.2 Compare with Other Models

We compared our model with Shaman's [18], from data source, compartment, parameter estimate and model construction. See the table below. Our simulation results persist the single peak pattern in the temperate region and predict other activity pattern in the subtropical and tropical regions which the other model cannot.

paper			Shaman's	OU
Data	Climate	source	National Land Data Assimilation System(NLDAS) project-2 data set (NCEP North American Region Reanalysis), 1979 - present	National Center for Environmental Prediction (NCEP) reanalysis (EOMF server), 1990 – 2009
		resolution	Hourly, US region, 0.125˚X0.125˚	Daily, Globally, 0.25˚X0.25˚
		variables	Specific Humidity(SH)	Temperature(T), Specific Humidity(SH), UV radiation
	Population	source		Gridded Population of the World Version 3 (GPWv3), 1995
		resolution		85˚N – 58˚S, 0.25˚X0.25˚
Flu Observation Report	Google Flu Trend (weekly ILI per 100000 people seeking medical attention)		Municipal scale of 115 cities	50 states
	CDC ILI+		Nationally, regionally	
Math Model	Compartment		Susceptible-Infectious-Recovered-Susceptible (SIRS)	Susceptible-Exposed-Infectious-Recovered-Susceptible (SEIRS)
	Parameters		α: the rate of travel-related import of influenza virus into the model domain	λ: total # of birth in a unit time μ: death rate $1/\eta$: average latent period
			D: mean infectious period	$1/\gamma$: average infectious period
			L: average duration of immunity	$1/\rho$: average period of temporary immunity
			$2 \le D \le 7$	$\mu = \lambda = 1/70\ year = 0.000039138, 1/\eta \approx 5$ $1/\gamma \approx 7$
			$2 \le L \le 10$	$1/\rho \approx 100$
			$0.8 \le R_{0min} \le 1.3$ $1.3 \le R_{0max} \le 4$	
	Transmission Rate $\beta(t)$		$\beta(t) = \frac{R_0(t)}{D}$	$\beta(t) = \frac{R_0(t)(\mu+\eta)(\mu+\gamma)}{\eta} \approx R_0(t)(\mu+\gamma) \approx \frac{R_0(t)}{D}$
	Reproduction Number $R_0(t)$		$R_0(t) = R_{0min} + (R_{0max} - R_{0min}) \times p(t)$	$R_0(t) = R_{0max} \times \frac{p(t)}{\max p(t)}$
	Scaling Factor $p(t)$		$p(t) = IVT_{SH}$	$p(t) = \frac{IVT_{SH} + IVS_T + HS_T}{3}$
			$IVT_{SH} = e^{-aq(t)}, a = 180, q(t) = SH(t)$	$IVT_{SH} = 5 \times e^{-\frac{(SH+c)^2}{0.9\times10^{-3}}}$ $IVS_T = 0.8 \times e^{-\frac{(T-T_{min})^2}{1000}}$ $HS_T = 0.01 + 0.7 \times \left(1 - e^{-\frac{(T-T_{opt})^2}{200}} U_1\right) + 0.8 \times \left(1 - e^{-\frac{(T-T_{opt})^2}{125}} U_2\right)$
	Model Equations		$\begin{cases} \frac{dS}{dt} = \frac{(N-S-I)}{L} - \beta(t)\frac{SI}{N} - \alpha \\ \frac{dI}{dt} = \beta(t)\frac{SI}{N} - \frac{I}{D} + \alpha \\ \frac{dR}{dt} = \frac{I}{D} - \frac{R}{L} \end{cases}$	SEIRS equation: $\begin{cases} \frac{dS}{dt} = \mu(N-S) - \beta\frac{SI}{N} + \rho R \\ \frac{dE}{dt} = \beta\frac{SI}{N} - (\mu+\eta)E \\ \frac{dI}{dt} = \eta E - (\mu+\gamma)I \\ \frac{dR}{dt} = \gamma I - (\mu+\rho)R \end{cases}$
				SIRS equation: $\begin{cases} \frac{dS}{dt} = \mu(N-S) - \beta(t)\frac{SI}{N} + \frac{R}{L} \\ \frac{dI}{dt} = \beta(t)\frac{SI}{N} - \left(\mu + \frac{1}{D}\right)I \\ \frac{dR}{dt} = \frac{I}{D} - \left(\mu + \frac{1}{L}\right)R \end{cases}$

Figure 4.4: Compare with Shaman's models [18]

Chapter 5

DATA

In order to implement SEIRS simulations, population data and climate data are required to create the risk factors for different locations across globe. Also the flu report data and estimate from the public health is also required for the validation and analysis of our model, which will be discussed in the last part of chapter 7.

For a better display, we derive the land-ocean cover, Figure 5.1, from ArcGIS to show the area and boundary of land which is slightly different from the population area. We only focus on the habitat region and will show our result over this background.

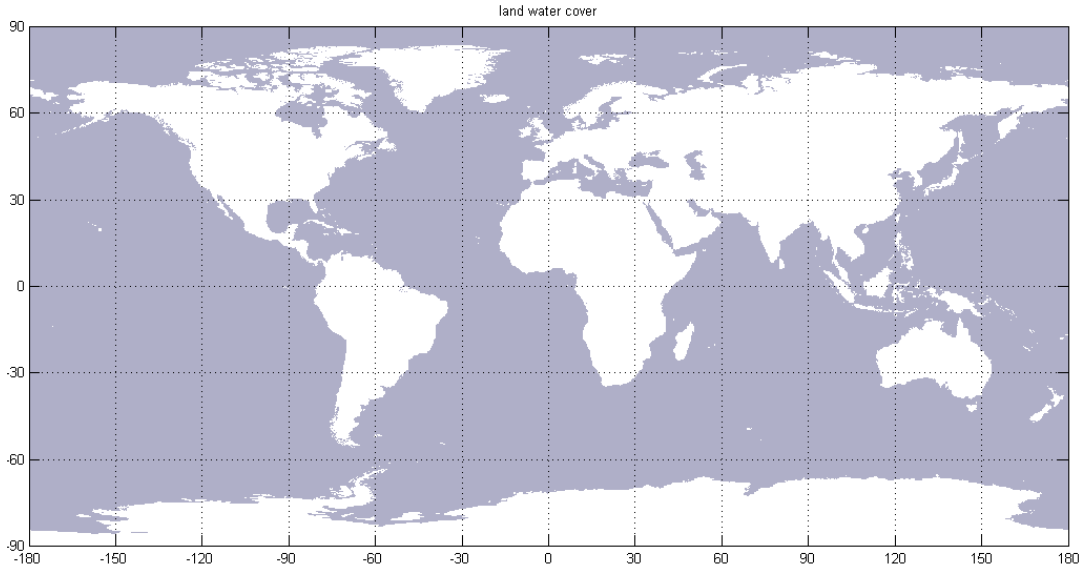

Figure 5.1: Land-Ocean boundary

5.1 Population

Human population data set is required in our model not only for the simulation but also to determine which areas need to be simulated, since we only considered human influenza circulation. The population data was obtained, from 1995 population count adjust to United Nations Gridded Population of the World, Version 3 (GPWv3) http://sedac.ciesin.columbia.edu/data/collection/gpw-v3, which offers 1995 population data on a 0.25 degree grid from 180° W to 180° E, 85° N to 58° S. Only the grid cells with the population greater than 0 needs to be paid attention to, see Figure 5.2.

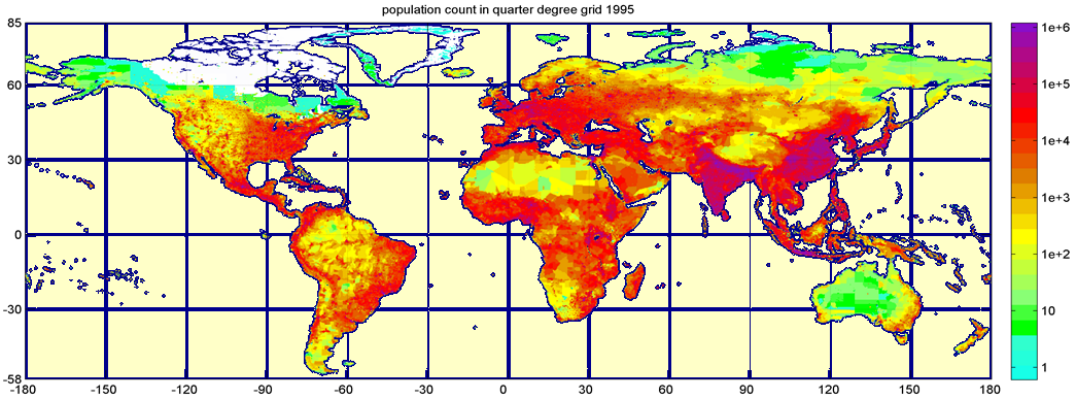

Figure 5.2: Human population in global scale (1995). Population data in the log scale value. Reddish color represents large population value, while blueish represents small amount of population.

5.2 Climate Data

- We obtained climate data (temperature and humidity) from the United States National Centers for Environmental Prediction (NCEP) http://www.esrl.noaa.gov/psd/data/gridded/reanalysis/, where offers monthly mean data from 1990 to present with 2.5 degree grid all cross the world. With interpolation, we got 0.25 degree resolution monthly data (180° W

to 180° E, 90° N to 90° S) for our simulation. Figure 5.3 is an example of the monthly mean temperature in January 1990.

- We also downloaded the daily climate data from NCEP with the same spatial resolution and converted data into the weekly mean according to the flu report schedule, in order to simulate weekly results. With this process, we are able to compare and validate our model with reported flu data.

5.3 Influenza Case Report Data

- US CDC weekly surveillance report (http://www.cdc.gov/flu/weekly/fluactivitysurv.htm).
- Google Flu Trend (GFT) (http://www.google.org/flutrends/), an open source estimation of the influenza activities in different scales: state, city, and region. The weekly estimation trace back to 2003 - 2004 flu season.
- China CDC weekly surveillance report (http://www.cnic.org.cn/).

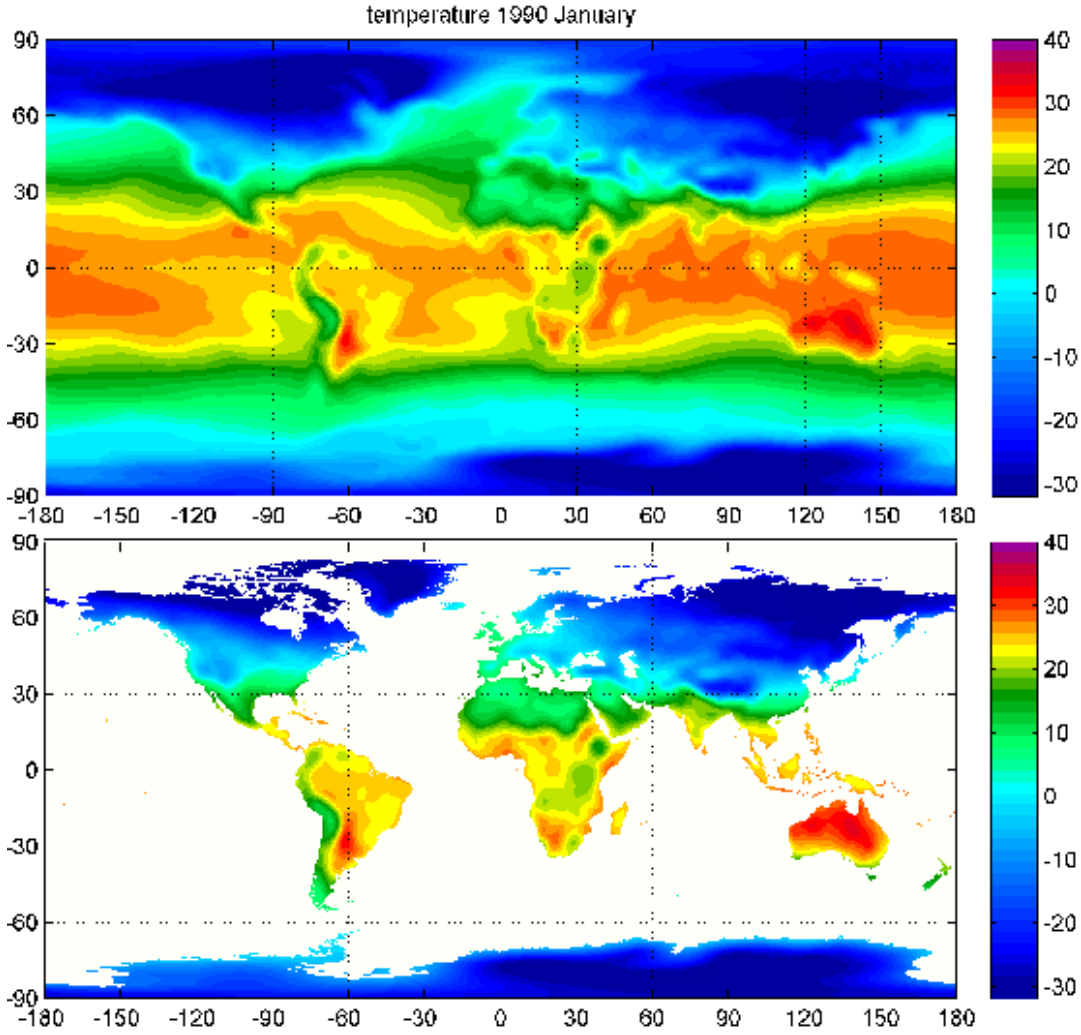

Figure 5.3: Global temperature in January 1990. The upper figure shows the monthly data obtained from NCEP, reddish color represents high temperature in Celsius degree, while blueish color represents low degree temperature. The lower figure shows the temperature data cropped into land cover shape with the same color scale as upper figure, with a blue cover represent the ocean area.

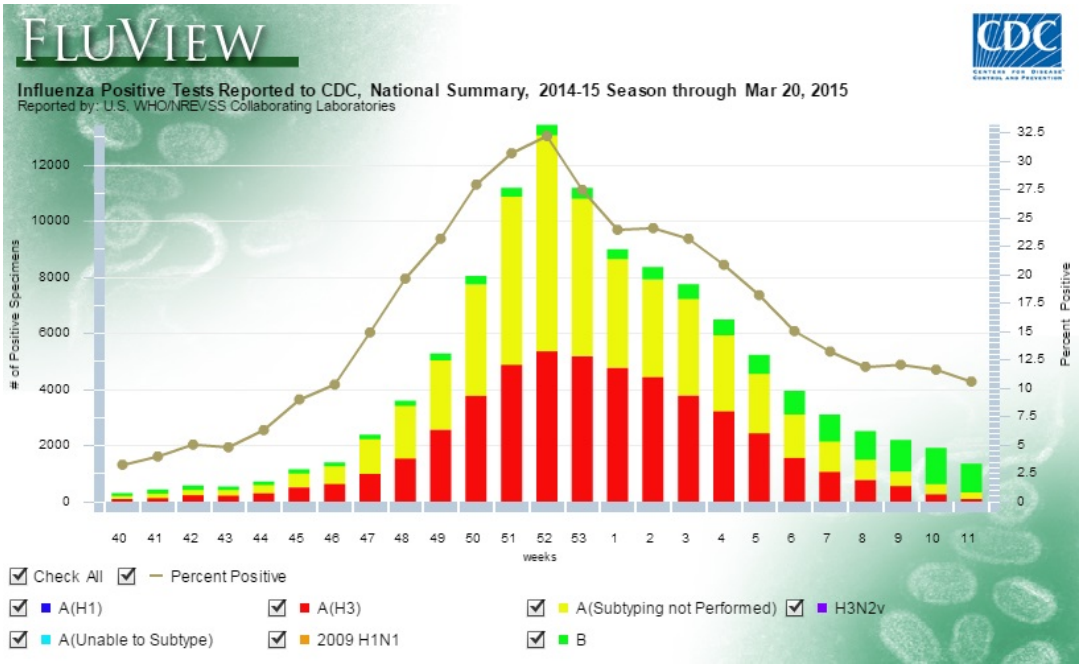

Figure 5.4: Flu View from US CDC, downloaded April 2nd, 2015

Chapter 6

Simulation

Our current study focused on simulating both single winter peak in the temperate region and double peak (summer–winter) in the subtropical region with one single model. The simulation results is compare with the patterns from the CDC observed data during the year 2006-2009.

1. Starting from single city sites (Beijing and HongKong, see Figure 7.1), check whether the simulation results produce the observed pattern.

2. Pick up multiple cities of 3 transects (North-South America, Europe-Africa and Russia-Asia-Australia, see Figure 7.2) and do the simulation, check if the flu activity pattern changed along the latitude gradient.

3. Then we extended our model simulations to the global scale and investigate the spatial distribution of flu activity across the world.

4. By classifying the flu pattern, we distinguished the source – sink regions [30] of the flu virus and explore possible flu transmission mechanism in different areas and help to better understand the circulation of flu.

5. Global simulation results are accumulated into city, state or countrywide to compare with GFT or CDC data. We compare the seasonal patterns and peak timing.

6. After monthly and weekly simulation, we compared our results with CDC influenza-like illness (ILI) case report number, which is weekly reported. GFT also contained weekly estimation on country, state and city. We used these to compare our result in different spatial scales.

Spatial pattern of influenza cases would also depend on other issues/factors, like landform, travelers and rainfalls. More investigations are required to calibrate our model.

6.1 Simulation Design

For each single point/grid cell in the data set, there are 20 years of humidity and temperature data associated with population numbers. We considered three response functions to construct a risk factor $p(t) = (IVT_{sh} + IVS_T + HS_T)/3$. When we plugged in the climate data with the time order, the risk factor p(t) become a function in terms of time. After estimating the parameter $\beta_0(t)$ by equation(4.5), all the information and data were ready for the simulation. In order to adjust the time increments in every step of the numerical method (Runge-Kutta 4th order), we also use spline method to interpolated the risk factor p(t) to make a smooth risk factor function respect to time over 20 years. Therefore, two more years were added to both the beginning and end of the data sequence to make sure the shape between 1990 and 2009 was well fitting. We suppose at the very beginning, a small portion of population is infected. Then we run the model and simulate the influenza circulation for several years before enter the time period with which we are especially concerned $(1990 - 2009)$. To do this, we add one more artificial year in front of our data to make an additional run cycle. Hence, in total there were three artificial years surrounding the real

data set, two in the front and one at the end. For convenient, we repeated the first year (1990) twice in front, and the last year (2009) once at the end. After the numerical simulation for a particular grid cell, we can plot a time dependent curve to show the flu activity change over the years for this grid cell.

6.2 Simulations at Single City

We choose two representative cities, one in temperate region (Beijing), one in subtropical region (Hong Kong) to test our hypothesis. Actually, cities in the temperate region experience very similar pattern, one strong winter epidemic peak and no flu activity during the summer time. For the subtropical cities, only a small region has the typical double peaks during one year, for example, the narrow strip around the southeast Asia.

6.3 Simulations at Multiple Cities along Latitudinal Transects

After the single city simulation with two different types of patterns, we consider whether our model work for a wide range of latitude and longitude. So we pick up 30 large cities along 3 transects: North /South America, Europe-Africa, and Russia-Asia-Australia. Along each transect, we choose a city in every 10 degree latitude range. In this way, we are able to see if the activity pattern change along the latitude gradient. The following two figures give the information of the 30 cities and show their locations in the map.

6.4 Simulations Across the World in OU Supercomputer

We also collected all the results from all the grid cells and display the global result by graphs and movies. For each time point, we collected all the results at

	North/South America					Europe - Africa					Russia – Asia - Australia				
	NO.	City	Country	Lat. Lon.	Pop. Elev.	NO.	City	Country	Lat. Lon.	Pop. Elev.	NO.	City	Country	Lat. Lon.	Pop. Elev.
50N	#1	Fairbanks	USA	64.84 -147.72	31535 136m	#11	Stockholm	Sweden	59.33 18.07	864324 21m	#21	St. Petersburg	Russia	59.95 30.32	4879566 13m
40N	#2	Montreal	Canada	45.50 -73.58	1649519 47m	#12	Madrid	Spain	40.40 -3.68	3273049 650m	#22	Harbin	China	45.80 126.67	5878939 141m
30N	#3	Oklahoma City	USA	35.48 -97.54	579999 366m	#13	Cairo	Egypt	30.06 31.23	6758581 26m	#23	Beijing	China	39.92 116.42	19612368 52m
20N	#4	Miami	USA	25.78 -80.18	2500625 2m	#14	El Aaiún	Western Sahara	27.15 -13.20	196331 23m	#24	Hong Kong	China	22.33 114.18	7061200 88m
10N	#5	Mexico City	Mexico	19.43 -99.13	8851080 2243m	#15	Dakar	Senegal	14.57 -17.48	1030594 30m	#25	Bangkok	Thailand	13.75 100.49	8249117 9m
0°	#6	Bogota	Colombia	4.60 -74.08	8958234 2561m	#16	Yaoundè	Cameroon	3.87 11.52	2440462 731m	#26	Singapore	Singapore	1.23 103.92	5183700 27m
10S	#7	Fortaleza	Brazil	-3.75 -38.58	2315116 29m	#17	Nairobi	Kenya	-1.28 36.82	3138295 1670m	#27	Bali	Indonesia	-8.33 115.00	3891428 0~3031m
20S	#8	Lima	Peru	-12.04 -77.03	7605742 119m	#18	Lusaka	Zambia	-15.42 28.28	1742979 1281m	#28	Darwin	Australia	-12.45 130.83	127532 19m
30S	#9	Sao Paulo	Brazil	-23.55 -46.63	11316149 733m	#19	Pretoria	South Africa	-25.75 28.19	525387 1320m	#29	Brisbane	Australia	-27.47 153.03	2074222 25m
40S	#10	Buenos Aires	Argentina	-34.60 -58.38	2891082 26m	#20	Cape Town	South Africa	-33.93 18.42	827218 12m	#30	Sydney	Australia	-33.86 151.21	4627345 37m

Figure 6.1: Information of 30 cities. The table lists the name, country, latitude, population and elevation of the cities of 3 transects, from north to south, along the latitude.

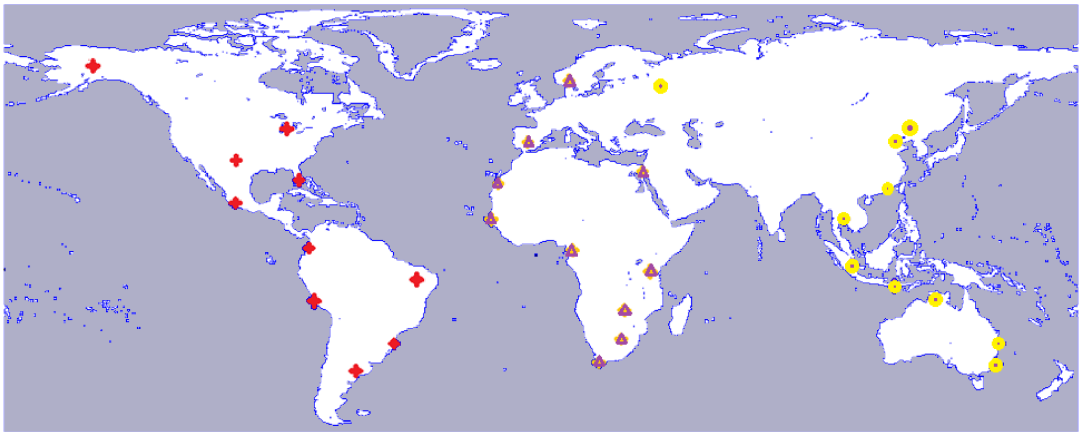

Figure 6.2: Marked locations of 30 cities in the map. '+', 'Δ', and '$\circ$' represent the 3 transects: North/South America, Europe – Africa and Russia – Asia – Australia, respectively.

this time from all the grid cells then created a graph of the flu activity at the certain time. Then all the frames placed in the time line create a movie of the flu activity over the human population across the whole world.

Consider the size of our data. On a $\frac{1}{4}$ degree grid for latitude and longitude globally, that is 4×180 (degree of latitude) $\times 4 \times 360$ (degree of longitude), about 1 million points need to be calculated and simulated. Even if we consider only inhabited sites, the data size is formidable, 250,000 or $\frac{1}{4}$ of the original size. We run our simulation in the Matlab environment. For each point, the simulation takes about 30 seconds. $\frac{1}{4}$ million points take about 3 months to finish by a single core computer! In practice, we used parallel computing with 8 cores (50 CPUs) to manipulate a relatively small sized data set to speed up the procedure so that it is accomplished within 10 hours. The quarter million points are divided into 50 data sets, each containing 5000 points. The results appear as 50 data sets that contain the result of the 20 years simulation for the world population areas. To display the results as a global map, we need to extract a selected time period result from the 50 sets, then combine them into one set and show the data in corresponding position.

6.4.1 Threshold

We obtain the epidemic threshold for peak timing and multi-peak [19] to classify the global pattern:

1. Peak time : the month/week with maximum reported cases in one calendar year

2. Epidemic threshold:

   Monthly: 5%, 10% of the total annual reported cases

Weekly: 1.2%

3. Epidemic period: case number above epidemic threshold

4. Multiple/Semi-annual peaks: two peaks $>$ 4 months apart, separated by a period with average case number below threshold

We use these criteria for both observed data and simulation results.

Chapter 7

Results

7.1 Single City

Our SEIRS simulation results have the single winter peak in the Beijing over 1990 - 2009 years by SEIRS model coupling with the NCEP monthly climatic data (temperature and specific humidity). The SEIRS model simulation also have the winter – summer double peak in the Hong Kong region in 1990 – 2009. These two cities results are coincident with the observation data [28, 38]. The response functions, risk factor, reproductive number and infectious fraction (I/N) of the two cities are shown below.

7.2 Multiple Cities along Latitudinal Transects

For the 3 transects, 30 cities were chosen along the latitude gradient. Along each transect, from north to south, we can observe the activity pattern from single peak, double peak, consistent and backward. The peak timing also shrifts along the latitude change. The magnitude of the incident fraction also change along with pattern change, with a high value in the temperate region and relative low rate in tropic. When we look horizontally, within the same latitude range, the flu activity patterns are similar.

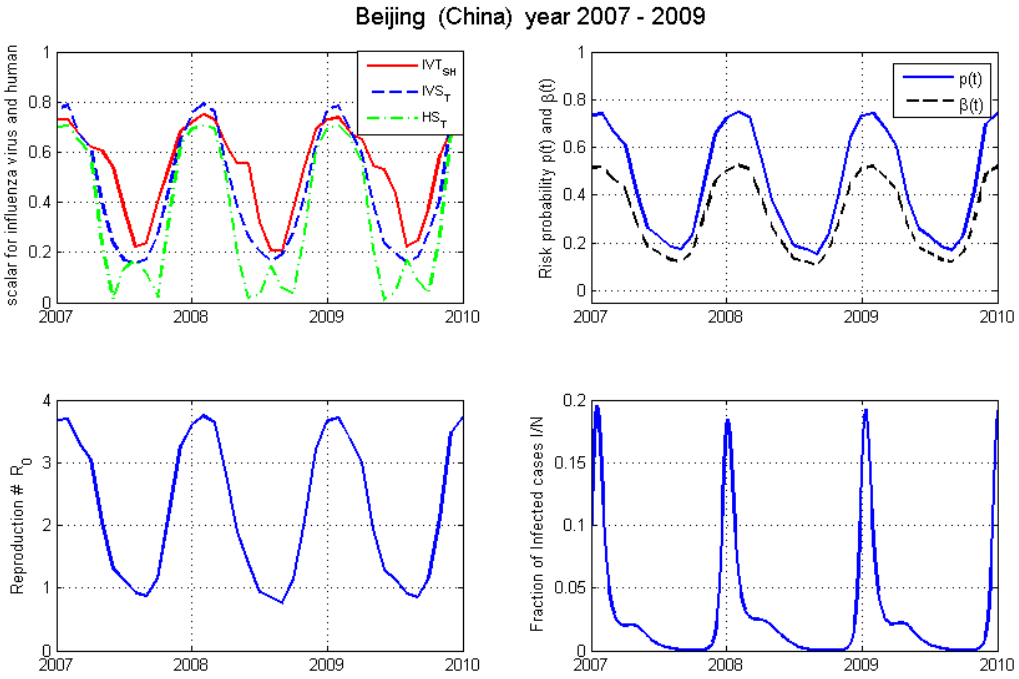

(a) Beijing

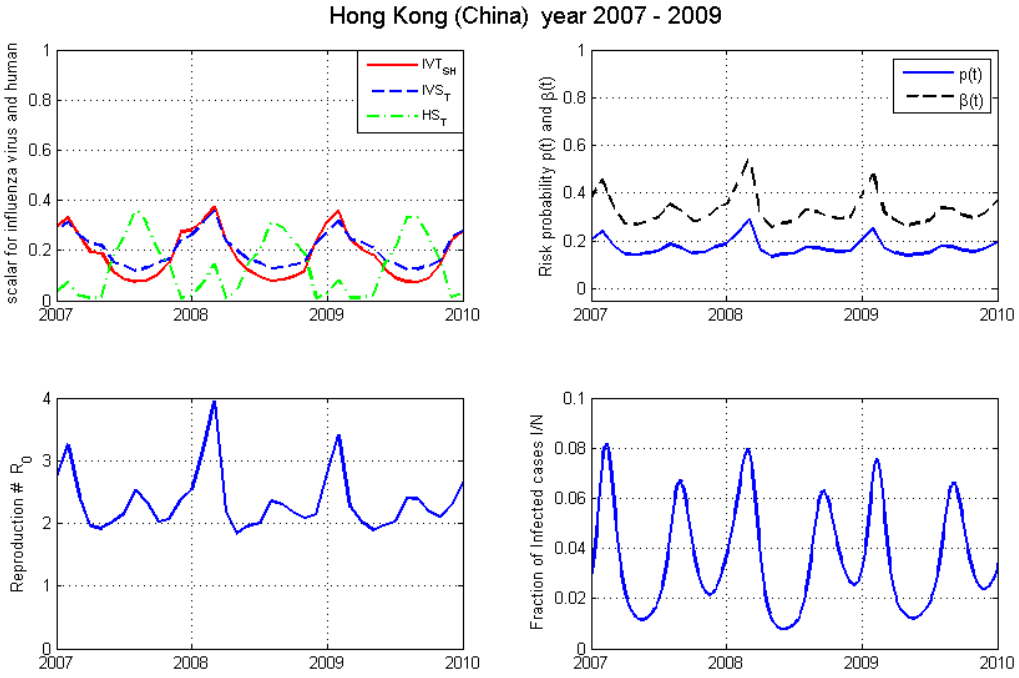

(b) Hong Kong

Figure 7.1: Response functions, Risk factor, Reproduction number and Simulation result of Beijing and Hong Kong cases

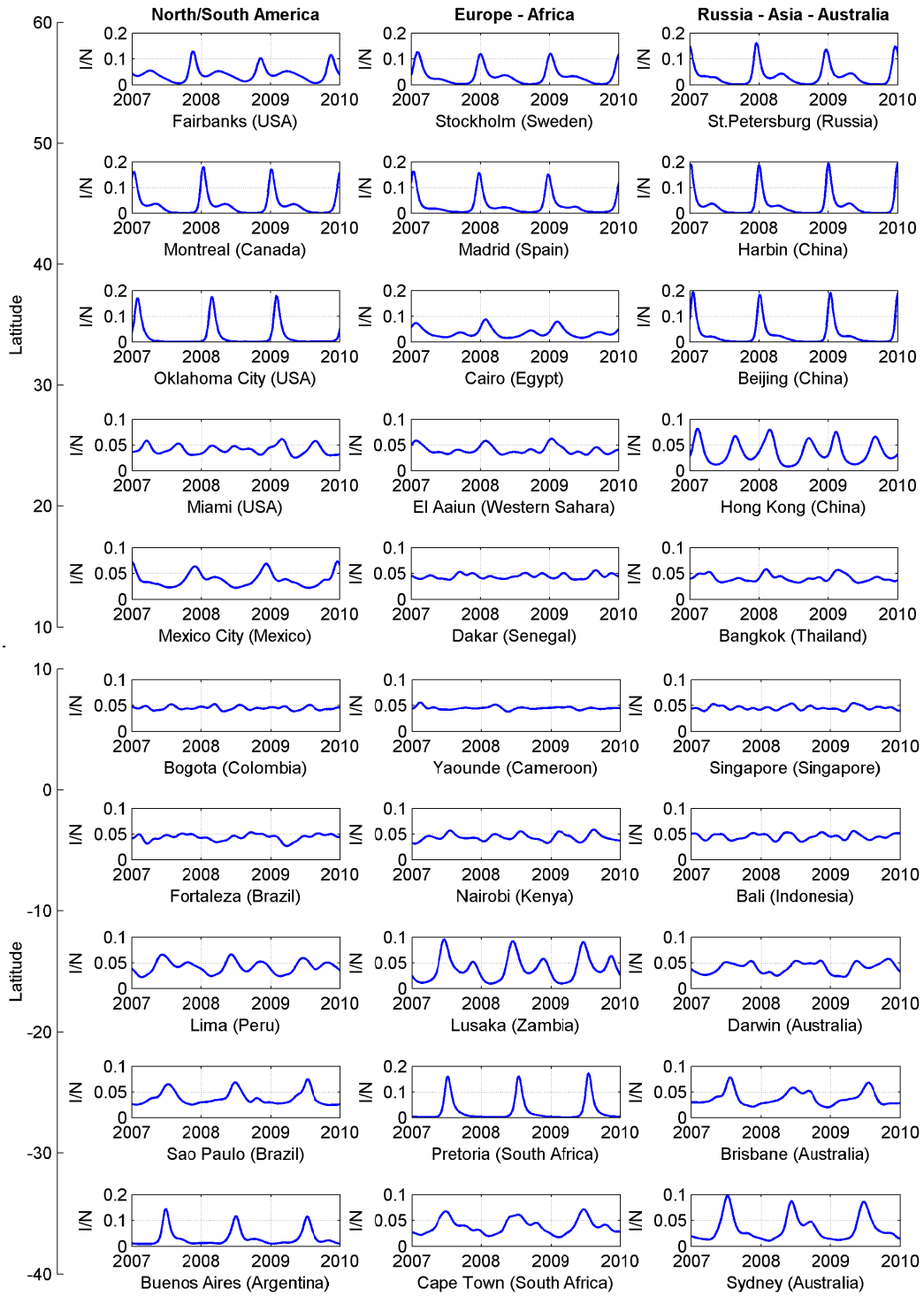

Figure 7.2: Influenza incident rates in 30 cities.

7.3 Global Scale

The global result shows the flu activity circulate through out the world. Starting from the cold zone and tropic region, flu virus maintains and transmits to the temperate region, occurs outbreak there in the local winter and vanished during the local summer time. The following figures show the maximum and minimum infectious fraction, the highest activity occurs in the northern temperate region, the cold zone and tropic region keep a high background level.

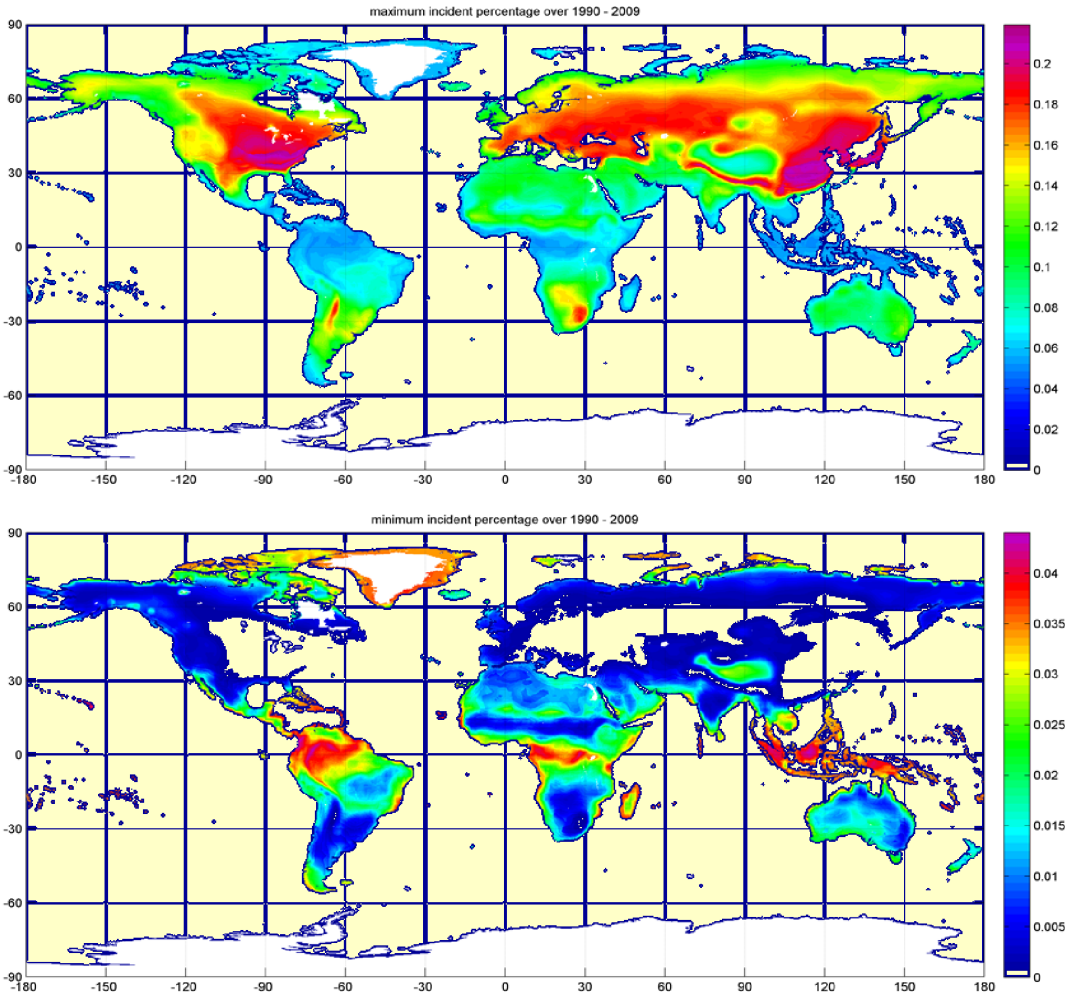

Figure 7.3: Maximum and minimum incident rate in global scale. Different latitude regions experience different patterns during the year.

We are able to classify the source and sink regions through out the globe with our global simulation: source area with persistence activity background, sink area with high fluctuation and vanish some time during the year, and the rest parts are the transition region. This result supports and enhances the source-sink hypothesis.

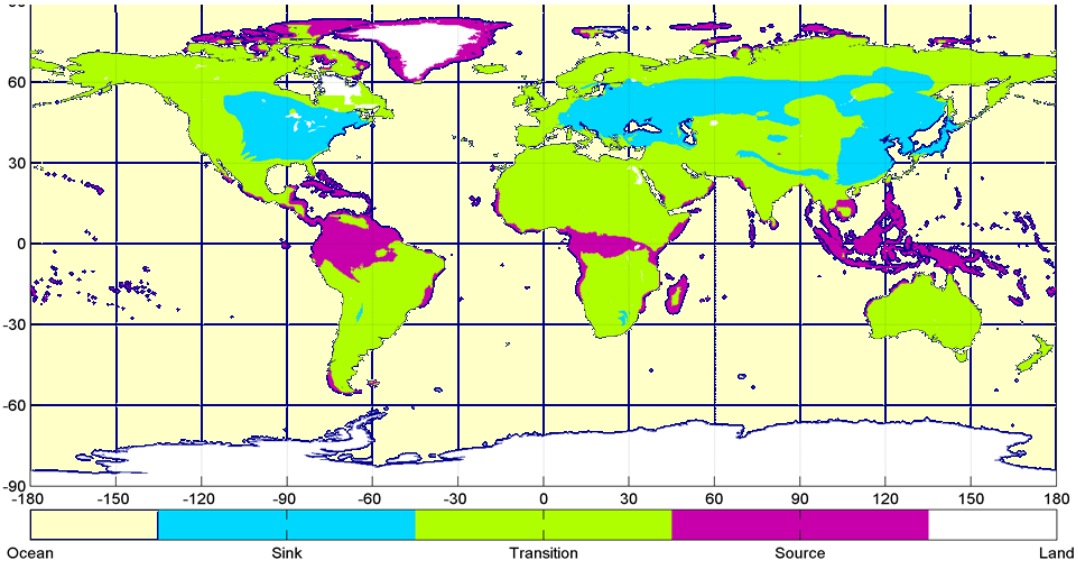

Figure 7.4: Predicted source and sink areas of influenza virus according to the incident rate. The source area contains a persistent rate along the year, while sink area has some period free of flu activity.

7.4 Validation

7.4.1 Compare with Google Flu Trend

We define the month/peak with the greatest infection fraction within a calender year as the peak month/week as in the subsection 6.4.1. Then we compare the peak timing of our simulation result with Google Flu Trend within the 50 states of US. As in the Figure 7.6, in the Google Flu Trend, different year has different peak time, all the states within the same year have similar peak time; on our

model, most the flu peak within 45 week to the 9 week for all the flu seasons from 2003 – 2009. There are 3 circles that indicate the region that our results close to the GFT result: most parts of the flu seasons 2003 – 2004, half parts of seasons 04 - 08 are fitted with the GFT results. For some early peak time, for example, the H1N1 avian flu in season 08 – 09, our model not able to detect the early peak before the 40th week.

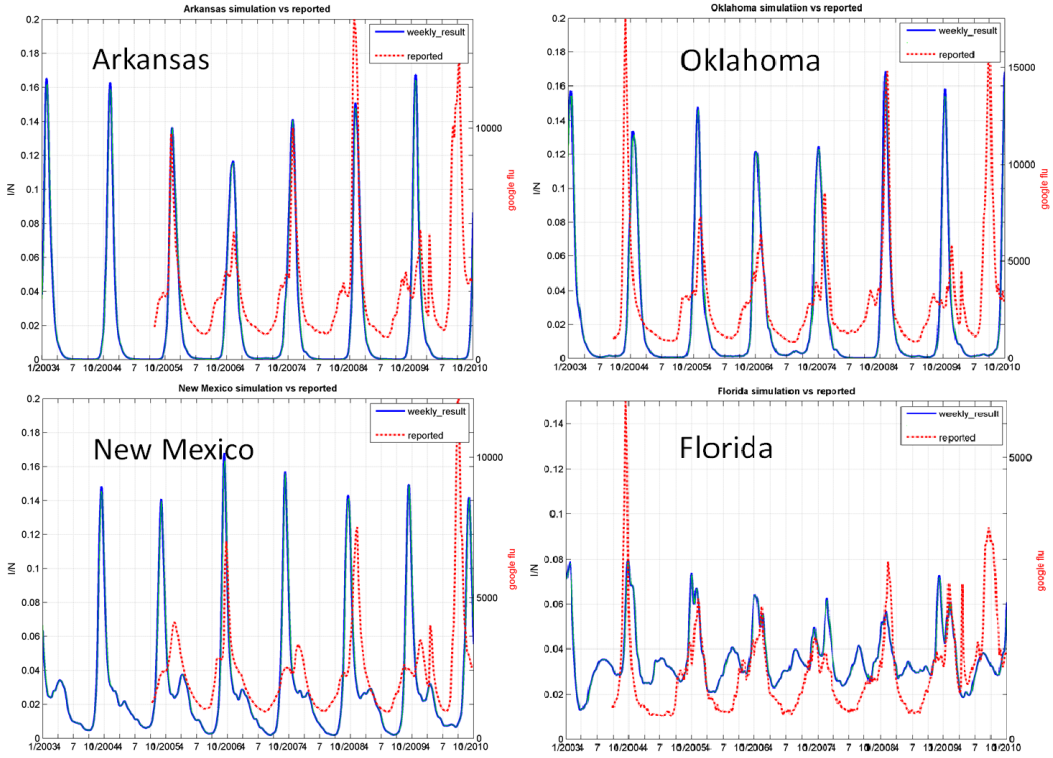

Figure 7.5: US cities results compare with Google Flu Trend

7.4.2 Compare with China CDC

We choose 11 cities along the east coast of China, almost one city per 2 latitude degree. Norther cities fit well, while southern cities meet variety types conditions I am not able to explain in this moment.

Aggregate the monthly grid point result into the north and south china, then

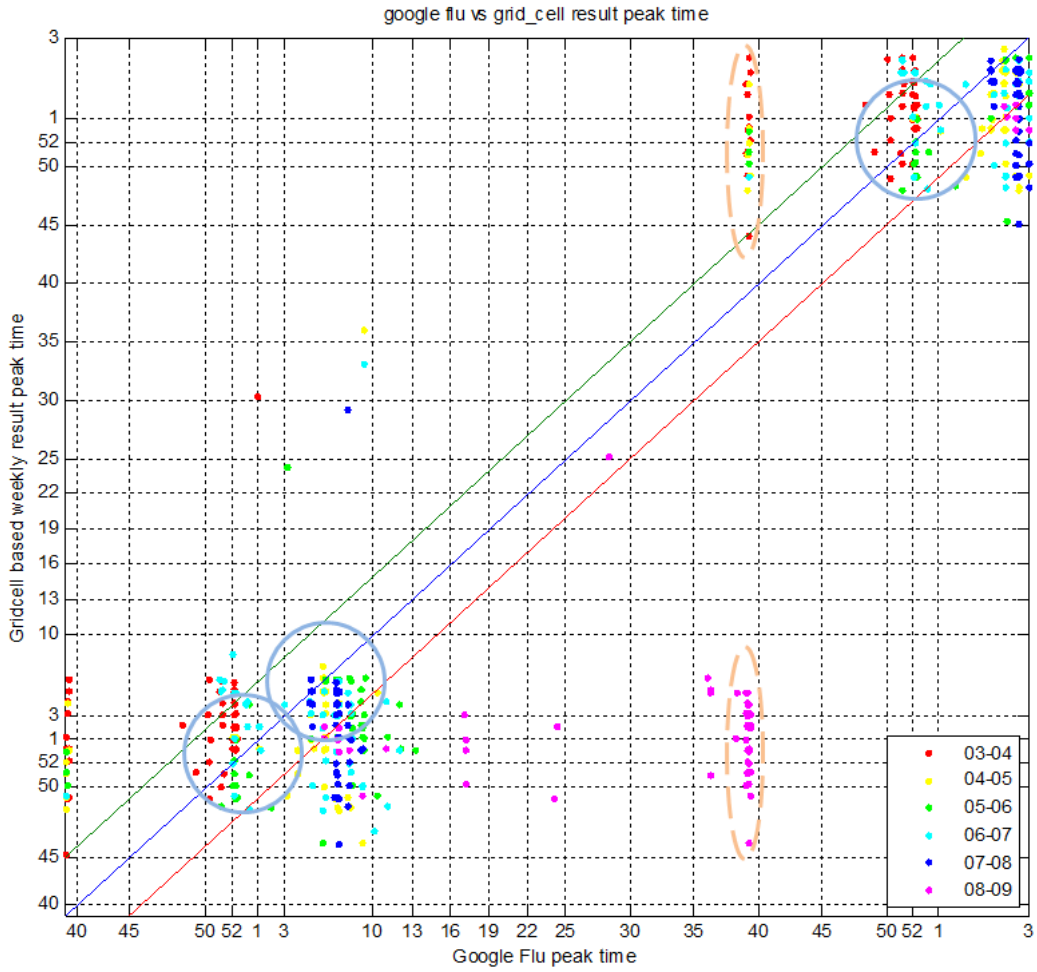

Figure 7.6: Compare flu activity peak time with Google Flu Trend estimation result for the 50 states of US, from season 2003 - 04, to season 2008 - 09. The scale number indicate the week of the year, from 40th week through out the next year, to the first 3 weeks of the third year.

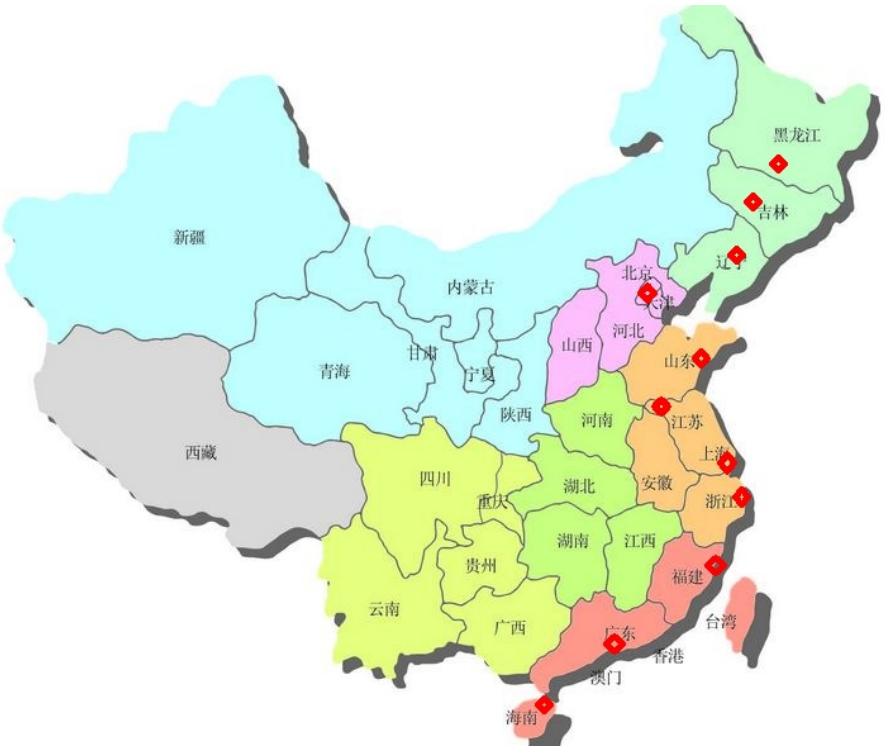

Figure 7.7: Location of 11 cities in China.

compare with China CDC ILI positive surveillance result. In the north part, our simulation result fixed the report; In the south part, we only product the winter peak.

7.5 Statistical Analysis

When the simulation result for the globe generated, we had a 20 years data in relation to the human population regions. It is great interest to find if there is any special pattern of the flu activity over the time and space. To explore this, we need to condense the huge data set into a small summarized brief set. For every grid cell, there are maximum, minimum and average values over 20 years, as well as annual maximum, minimum and average. We divided the summarized data set into 29 bins along latitude line, each bin containing results from a 5

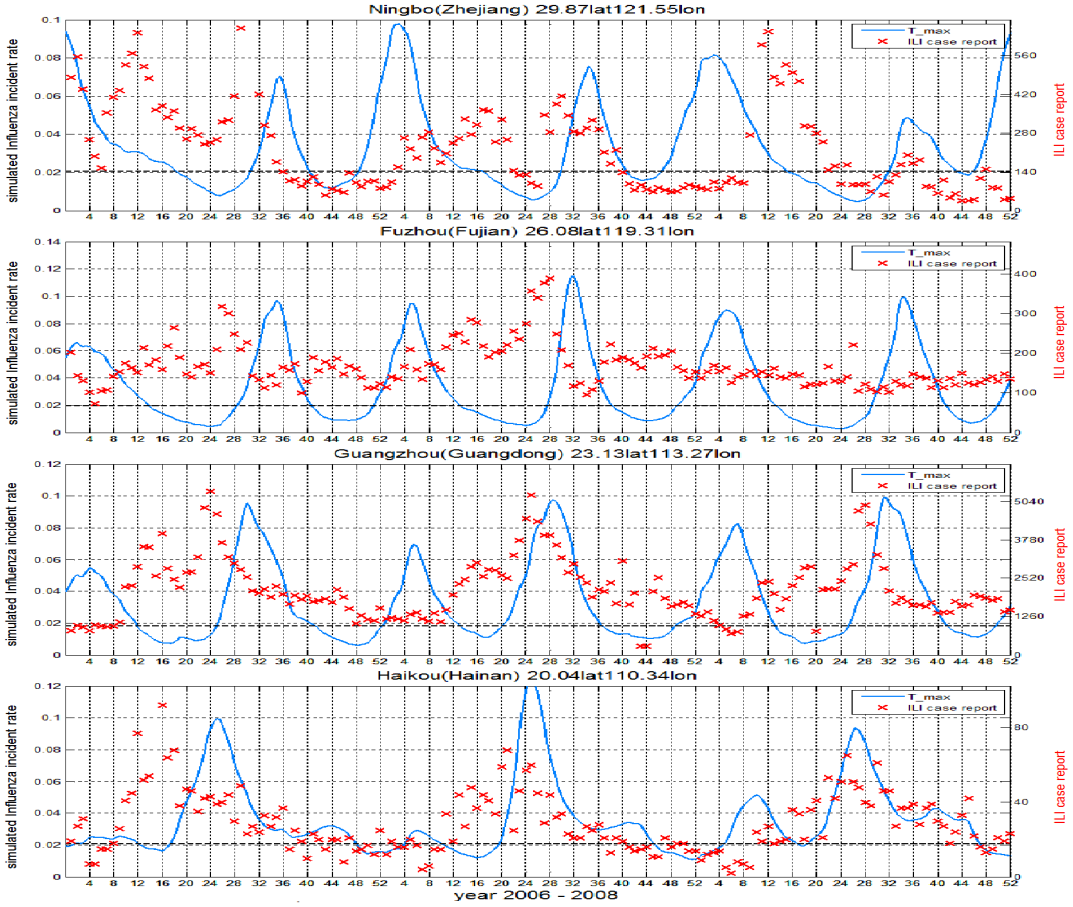

Figure 7.8: Compare result of cities in southern China.

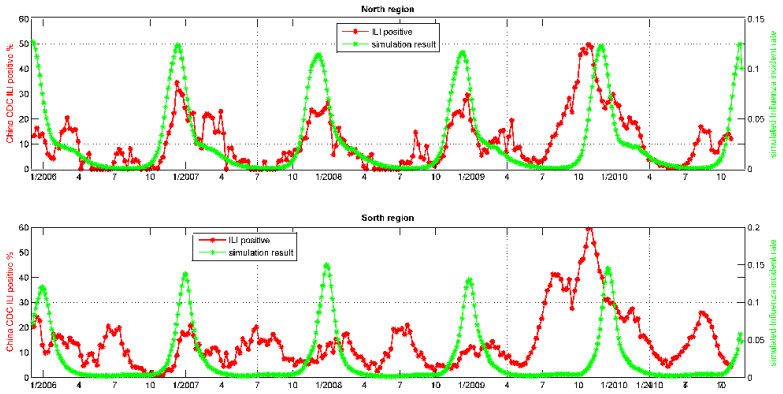

Figure 7.9: Simulation result compare with the China CDC ILI+ observation.

degree latitude region, performed statistical analysis over these bins and showed them along a latitude gradient. This process showed us a numerically significant difference across the world from North to South. Also, we can divide the results along longitude which showed the spatial distribution from East to West. By mathematical definition of the peaks, we also can create a map of the flu activity pattern across the world, see Figure 7.4.

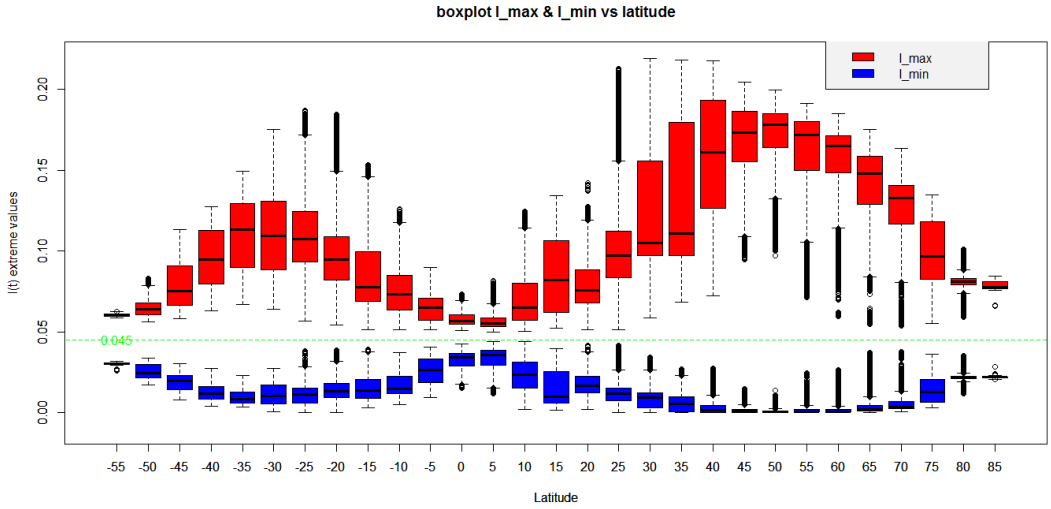

Figure 7.10: Max and min incident rate along latitude gradient.

In order to analyze the spatial properties of flu activity through 20 years, we needed to deal with the result sets first, finding the maximum and minimum over the 20 year simulation for each point we calculated [Figure 7.3]. By showing the graph of the extreme value for each point, we constructed a map to visualize the global pattern of influenza epidemiology. Also, we constructed a standard for the source/sink based on the multiple cities result to identify the source/sink area and flu activity pattern.

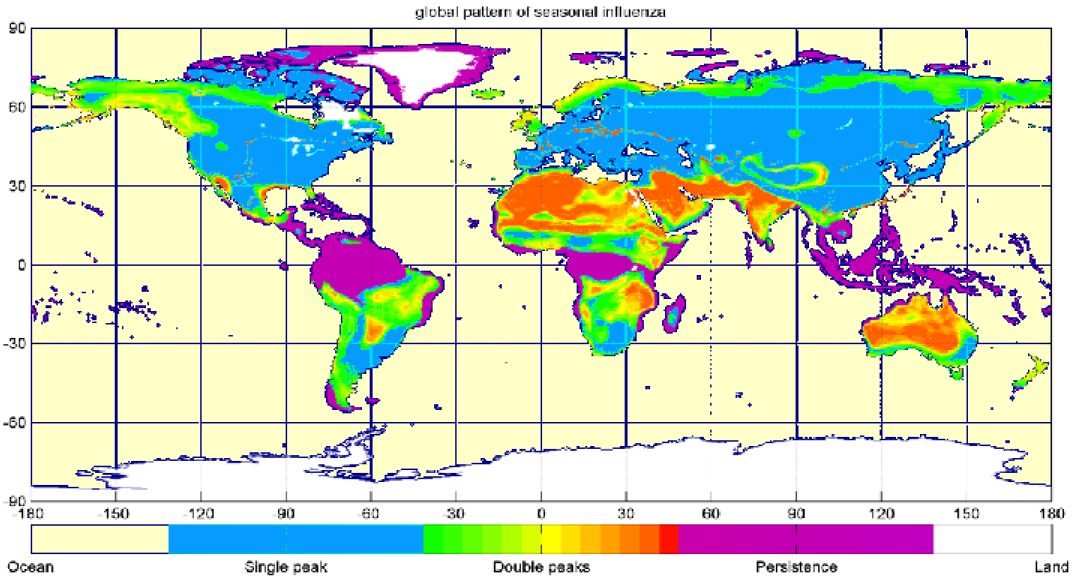

Figure 7.11: Spatial patterns of seasonal dynamics of human influenza in the world. By the same definition of single/double peaks we used in the multiple cities case, we classified three areas based on their seasonal dynamics of influenza.

Chapter 8

Discussion

From the 30 cities simulation results, we can see that the seasonality patterns change along the latitude gradient. In both North and South moderately high latitude (temperate) regions, there is one flu epidemic peak in the local winter. The magnitude of the incidence ratio is close to 10%. In the subtropical regions, there is more than one peak during a single year, and the highest incidence rate appears in the local winter or rainy season and is lower than the peak in the temperate regions. In the tropics, flu activity fluctuates all year round with the magnitude of incidence very close to 5%, which is almost half value of the temperate areas. In the temperate areas, influenza vanishes during local summer, but in the cold and tropical zones it persists all through the year. Thus, we see a variation along the lines of latitude, but almost no change along the lines of longitude.

From our global simulation, we can see almost the same results as we obtained from multiple cities result: a high activity ratio in the temperate zone and a low ratio in the tropics. Even more, we also can see the seasonal pattern among and outside the regions that had been fully discussed above. Flu activity rates changes to a large extent along the lines of latitude, but really small changes on the longitude gradient. The relatively low and persistent rate in the high latitude region suggests a source in the cold zone.

From the flu activity of a single city, it is easy to see how flu peaks, vanishes

or persists along a timeline. Then considering a list of cities along the latitude line, each city has its own flu peak time, duration and strength. Put the above information of multiple cities in one figure, we can see the flu transfers from one place to another along the latitude according to time, and the flu peak ratio change according to the space. If we collect and display all the flu activity over the world for a single year, we will see influenza outbreaks shift from the cold zones and the equator to temperate areas and then go back. The annual spatial pattern indicates the yearly flu movement from source to sink. In cold and tropical regions, influenza fluctuates very little and transmits to the nearby areas all year round. In the temperate regions, influenza peaks with relatively high ratio during the local winter and vanishes during the summer. In the areas between the above regions, there may be several peaks with moderate ratio values during one year[Figure 7.2].

Chapter 9

Future Work

- So far, we are able to simulate the seasonal dynamics pattern in many cities and fit the observations. However, comparing to China CDC report, simulation results did not fit the peak timing well, usually several weeks ahead. For some particular cities, the observation didn't follow the classical patterns that we summarized. Some other factors may play the important roles in the flu transmission other than the climate factors, for example, vocation season, air condition, sport events and so on. We need to consider local issues, since the flu pattern is highly depended on the human activities.

- In order to compare the magnitude, we need a scale to actually compare the simulation and observation. The pattern actually fix well in both North and South cities in China. We need more observation reports to calibrate our result and then extend our model to the global scheme. Our model is a rough idea, more consideration should be taken into account.

- To validate the simulation results, besides comparing peak timing and magnitude, other tools and methods are required to measure the relation between two time sequences.

- It requires more work and research to figure out which observation report can represent the infected group activity, ILI (Influenza Like Illness) cases

or ILI+ (ILI positive tested) cases.

- All the parameters in the mathematical model have their ranges. Different location may required different values of parameters. Improving our results by choosing the best fit parameters in the ODE models according to the spatial location is one important step next.

- Our global spatial pattern actually is come from the spatial variation of the input data. It is possible to consider a relation of climate data and flu outbreak out of our simulation result.

- Also, introduce the diffusion terms to describe the environment/social effects involved in the flu transmission due to the spatial influence.

9.1 More Risk Factors

In the next step, we will consider the fourth risk factor, human susceptibility in terms of UV radiation, HS_{uv}, and modifying the risk factor as $p(t) = p_4(t) = (IVS_SH + IVT_T + HS_T + HS_{rad})/4$. We could do the same simulations with the new risk factor $p_4(t)$ and compare these results with the results we have already obtained from the three response functions. We will also compare the simulation results with real data to check if there is any possible mechanism or model that can describe this seasonality more efficiently in order to modify and improve our procedures. Our study gives a better understanding of the flu circulation and will help the government to make decision about the disease control.

9.2 PDE Models

In the current model, we assume a uniform distribution of infected population in given location. The distance between individuals should play an important role in the contact and transmission. In the future work, we want to introduce the diffusion term to describe the local spatial influence to the flu activity. Also, social activity would affect our model, since people propagate in local events, such as football games, festival gala, parade and other kind of celebration.

In the future, we will consider SEIRS model with additional diffusion term to the transmission process to describe the spatial transmission factor: $k_1\Delta S$, and $k_2\Delta I$.

$$\begin{cases} \frac{dS(t)}{dt} &= k_1\Delta S + \lambda - \mu S(t) - \beta(t)\frac{S(t)I(t)}{N(t)} + \rho R(t) \\ \frac{dE(t)}{dt} &= \eta E(t) - (\mu+\gamma)I(t) \\ \frac{dI(t)}{dt} &= k_2\Delta I + \beta(t)\frac{S(t)I(t)}{N(t)} - (\mu+\eta)E(t) \\ \frac{dR(t)}{dt} &= \gamma I(t) - (\mu+\rho)R(t) \end{cases} \tag{9.1}$$

9.3 Spatial Analysis

All the reports and estimation data come from local health department or website can be classify and give further conclusion according to the spatial location. We also did this type of spatial analysis to our simulation results. We did verification to our result in the spatial scale and can move forward from the analysis discussion.

9.4 Age Groups

Consider the age structure of the local population, different age people have different risk probabilities in the flu circulation process. So divided each component into several age groups will improve our model to a new stage. Also we need to consider the transmission among and between groups, which involves a great number of parameters which should be estimated from the real report and require further investigate.

Bibliography

[1] Lawrence C. Evans, *Partial Differential Equation: Second Edition (Graduate Studies in Mathematics)*, American Mathematical Society, 2010.

[2] Haim Brezis and Louis Nirenberg, *Positive solutions of nonlinear elliptic equations involving critical sobolev exponents*, Communications on Pure and Applied Mathematics. July 1983, Volume 36, Issue 4, pages 437C477.

[3] Michael Struwe, *Variational Methods: Application to Nonlinear Partial Differential Eqiations and Hamiltonian Systems*, Second Edition, Springer-Verlag, reprinted 2000.

[4] J. Moser, *A sharp form of an inequality by N. Trudinger*, Indiana Univ. Math. J. 11(1971), 1077-1092.

[5] Ni, Yilong, *The mean field equation with critical parameter in a plane domain*, Differential Integral Equations 19 (2006), no. 12, 1333–1348.

[6] Robert Whitley, *An Elementary Proof of the Eberlein-Smulian Theorem*, Mathemacische Annalen, 1967, Volume:172, page 116-118.

[7] Suyu Li, *Some Sharp Inequalities Related to Moser-Trudinger-Onofri Inequality*, 2014, University of Oklahoma, 55 pages.

[8] WHO.2014, available: http://www.who.int/mediacentre/factsheets/fs211/en/. Obtained April 10th, 2015.

[9] Fuhrmann, C., *The Effects of Weather and Climate on the Seasonality of Influenza: What We Know and What We Need to Know*, Geography Compass, 2010. 4/7(10.1111/j.1749-8198.2010.00343.x): p. 718–730.

[10] Liang Mao, Yang Yang, Youliang Qiu and Yan Yang, *Annual economic impacts of seasonal influenza on US counties: Spatial heterogeneity and patterns*, International Journal of Health Geographics 2012, 11:16 doi:10.1186/1476-072X-11-16.

[11] Park , A.W. and K. Glass, *Dynamic patterns of avian and human influenza in east and southeast Asia*. Lancet Infectious Diseases, 2007. 7(8): p. 543-548.

[12] Cohen, J., *Past pandemics provide mixed clues to H1N1s next moves*. Science, 2009. 324: p. 996-997.

[13] Dushoff, J., et al., *Dynamical resonance can account for seasonality of influenza epidemics*. Proceedings of the National Academy of Sciences of the United States of America, 2004. 101(48): p. 16915-16916.

[14] Tamerius, J., et al., *Global Influenza Seasonality: Reconciling Patterns across Temperate and Tropical Regions*. Environmental Health Perspectives, 2011. 119(4): p. 439-445.

[15] Shaman, J. and M. Kohn, *Absolute humidity modulates influenza survival, transmission, and seasonality*. Proceedings of the National Academy of Sciences of the United States of America, 2009. 106(9): p. 3243-3248.

[16] Shaman, J., Pitzer, V.E, Viboud, C, Grenfell, B.T, Lipsitch, M *Absolute Humidity and the Seasonal Onset of Influenza in the Continental United States*. PLoS Biology, 2010. 8(2): p. 1-13.

[17] Shaman, J., et al., *Absolute Humidity and the Seasonal Onset of Influenza in the Continental United States*. Plos Biology, 2010. 8(2).

[18] Shaman, J., et al., *Real-time influenza forecasts during the 2012-2013 season*. Nature Communications, 2013. 4.

[19] Bloom-Feshbach K, Alonso WJ, Charu V, Tamerius J, Simonsen L, et al. *Latitudinal Variations in Seasonal Activity of Influenza and Respiratory Syncytial Virus (RSV): A Global Comparative Review*. PLoS ONE 2013, 8(2): e54445. doi:10.1371/journal.pone.0054445

[20] Breban, R. (2013) *Role of environmental persistence in pathogen transmission: a mathematical modeling approach*. Journal of Mathematical Biology, 66: 535-546.

[21] Lowen, A.C., et al., *Influenza virus transmission is dependent on relative humidity and temperature*. Plos Pathogens, 2007. 3(10): p. 1470-1476.

[22] Chao, D.L., *Modeling the global transmission of antiviral-resistant influenza viruses*. Influenza and Other Respiratory Viruses (2013)7: 58-62.

[23] HOPESIMPSON, R., *The Role of Season in the Epidemiology of Influenza*. Journal of Hygiene, 1981. **86**(1): p. 35-47.

[24] Cannell, J., et al., *Epidemic influenza and vitamin D*. Epidemiology and Infection, 2006. 134(6): p. 1129-1140.

[25] Lowen, A.C., et al., *High temperature (30 degrees C) blocks aerosol but not contact transmission of influenza virus*. Journal of Virology, 2008. 82(11): p. 5650-5652.

[26] Chew, F., Doraisingham, S., Ling, A., Kumarasinghe, G., Lee, B. *Seasonal trends of viral respiratory tract infections in the tropics*. Epidemiology and Infection(1998) 121: 121-128.

[27] Dosseh, A., Ndiaye, K., Spiegel, A., Sagna, M., Mathiot, C. *Epidemiological and virological influenza survey in Dakar, Senegal: 1996-1998*. American Journal of Tropical Medicine and Hygiene(2000) 62: 639-643.

[28] Chan, P., Mok, H., Lee, T., Chu, I., Lam, W., et al. *Seasonal Influenza Activity in Hong Kong and its Association With Meteorological Variations*. Journal of Medical Virology(2009) 81: 1797-1806.

[29] Pulliam, H.R., *Sources, Sinks, and Population Regulation*. American Naturalist (1988)132: 652-661

[30] Rambaut A, Pybus OG, Nelson MI, Viboud C, Taubenberger JK, Holmes EC. *The genomic and epidemiological dynamics of human influenza A virus*. Nature. 2008 May 29; 453(7195):615-9.

[31] Maria C.A. Leite, Shiyun Tang, Xiangming Xiao, Meijun Zhu, *Prediction seasonal dynamics of human influenza along hte latitudinal gradient*. In preperation.

[32] Matt J. Keeling and Pejman Rohani, *Modeling Infectious Diseases in Humans and Animals*. Priceton University Press, 2008.

[33] wikipedia April, 2015,http://en.wikipedia.org/wiki/Compartmental_models_in_epidemiology

[34] Tuite, A.R., Greer, A.L.,Whelan, M.,Winter, A.-L., Lee, B., Yan, P., et al *Estimated epidemiologic parameters and morbidity associated with pandemic H1N1 influenza*. CMAJ, 2010. 182(2): p. 131-136.

[35] Velasco-Hernandez, J., Leite, M.C.A, *A model for SEIR diseases with social isolation*. Salud Publica de Mexico, 2011. 53(1): p. 40-47.

[36] Cannell, J., et al., *On the epidemiology of influenza*. Virology Journal, 2008. 5.

[37] Hartley, Anne, *"Fuel Poverty". West Midlands Public Health Observatory*. Birmingham, UK: West Midlands Public Health Observatory(1 March 2006), Page 3.

[38] Chinese National Influenza Center, http://www.cnic.org.cn/.